galaxies

IMPACT FACTOR 3.8

CITESCORE 6.3

Article

Early Optical Follow-Up Observations of *Einstein Probe* X-Ray Transients During the First Year

Siyu Wu, Ignacio Pérez-García, Alberto J. Castro-Tirado, Youdong Hu, Maria Gritsevich, María D. Caballero-García, Rubén Sánchez-Ramírez, Sergiy Guziy, Emilio J. Fernández-García, Guillermo García Segura et al.

Special Issue

Gamma-Ray Bursts in Multiwavelength: Theory, Observational Correlations and GRB Cosmology

Edited by

Dr. Maria Giovanna Dainotti and Prof. Dr. Nissim Fraija

MDPI

https://doi.org/10.3390/galaxies13030062

galaxies

MDPI

Article

Early Optical Follow-Up Observations of *Einstein Probe* X-Ray Transients During the First Year

Siyu Wu [1,2], Ignacio Pérez-García [1], Alberto J. Castro-Tirado [1,3,*], Youdong Hu [4], Maria Gritsevich [5,6,7], María D. Caballero-García [1], Rubén Sánchez-Ramírez [1], Sergiy Guziy [1,8], Emilio J. Fernández-García [1], Guillermo García Segura [1,9], Carlos Pérez-del-Pulgar [3], Dingrong Xiong [10] and Bin-Bin Zhang [11,12]

1 Instituto de Astrofísica de Andalucía, Consejo Superior de Investigaciones Científicas (IAA-CSIC), Glorieta de la Astronomía, s/n, 18080 Granada, Spain; wusiyu.11@outlook.com (S.W.); ipg@iaa.es (I.P.-G.); mcaballero@iaa.es (M.D.C.-G.); ruben@iaa.es (R.S.-R.); gssgrb@gmail.com (S.G.); emifdez@iaa.es (E.J.F.-G.); ggs@astro.unam.mx (G.G.S.)
2 Department of Physics and Mathematics, University of Granada, 18012 Granada, Spain
3 Departamento de Ingeniería de Sistemas y Automática, Unidad Asociada al CSIC por el IAA, Escuela de Ingenierías Industriales, Universidad de Málaga, C. Dr. Ortiz Ramos s/n, 29071 Málaga, Spain; carlosperez@uma.es
4 School of Physical Science and Technology, Guangxi University, 100 East Daxue Road, Xixiangtang, Nanning 530004, China; huyoudong072@hotmail.com
5 Swedish Institute of Space Physics (IRF), Bengt Hultqvists Väg 1, 981 92 Kiruna, Sweden; maria.gritsevich@helsinki.fi
6 Faculty of Science, University of Helsinki, Gustaf Hallströmin Katu 2, FI-00014 Helsinki, Finland
7 Institute of Physics and Technology, Ural Federal University, Mira Str. 19, 620002 Ekaterinburg, Russia
8 Petro Mohyla Black Sea National University, 54000 Mykolaiv, Ukraine
9 Instituto de Astronomía de Ensenada, Universidad Nacional Autónoma de México, Ensenada 22860, Baja California, Mexico
10 Yunnan Observatories, Chinese Academy of Sciences, 396 Yangfangwang, Guandu District, Kunming 650216, China; xiongdingrong@ynao.ac.cn
11 School of Astronomy and Space Science, Nanjing University, 163 Xianlin Road, Nanjing 210023, China; bbzhang@nju.edu.cn
12 Key Laboratory of Modern Astronomy and Astrophysics, Nanjing University, Ministry of Education, Nanjing 210023, China
* Correspondence: ajct@iaa.es

Abstract: We present early follow-up observations of *Einstein Probe* (*EP*) X-ray transients, following its first year of operation. *EP* is a dedicated wide-field X-ray observatory that is transforming our understanding of the dynamic X-ray universe. During its first year, *EP* successfully detected a diverse range of high-energy transients—including gamma-ray bursts (GRBs), tidal disruption events (TDEs), and fast X-ray transients (FXTs), besides many stellar flares, disseminating 128 alerts in the aggregate. Ground-based optical follow-up observations, particularly those performed by our BOOTES telescope network, have played a crucial role in multi-wavelength campaigns carried out so far. Out of the 128 events, the BOOTES Network has been able to follow up 58 events, detecting 6 optical counterparts at early times. These complementary optical measurements have enabled rapid identification of counterparts, precise redshift determinations (such as EP250215a at $z = 4.61$), and detailed characterization of the transient phenomena. The synergy between *EP*'s cutting-edge X-ray monitoring and the essential optical follow-up provided by facilities, such as the above-mentioned BOOTES Global Network or other Spanish ground-based facilities we have access to, underscores the importance and necessity of coordinated observations in the era of time-domain and multi-messenger astrophysics.

Keywords: *Einstein Probe;* X-ray transients; follow-up observations; gamma-ray bursts

Academic Editor: Stefano Bianchi

Received: 17 March 2025
Revised: 12 May 2025
Accepted: 13 May 2025
Published: 19 May 2025

Citation: Wu, S.; Pérez-García, I.; Castro-Tirado, A.J.; Hu, Y.; Gritsevich, M.; Caballero-García, M.D.; Sánchez-Ramírez, R.; Guziy, S.; Fernández-García, E.J.; García Segura, G.; et al. Early Optical Follow-Up Observations of *Einstein Probe* X-Ray Transients During the First Year. *Galaxies* **2025**, *13*, 62. https://doi.org/10.3390/galaxies13030062

1. Introduction

X-ray transients represent some of the most energetic and dynamic phenomena in the universe, offering unique insights into extreme physics and fundamental astrophysical processes [1–3]. These events encompass a diverse range of sources, including tidal disruption events (TDEs), gamma-ray bursts (GRBs), stellar flares, and compact object mergers [4]. While X-ray observations reveal their prompt emission mechanisms, optical follow-up observations play a pivotal role in classifying transients, measuring redshifts, and constraining multi-wavelength energetics. For example, optical spectroscopy provides critical redshift measurements for cosmological GRBs [5], while color evolution in afterglows probes jet dynamics and circumburst environments [3].

The *Einstein Probe* (EP) mission [6,7] addresses the need for wide-field X-ray monitoring with its unique dual-telescope design: the Wide-field X-ray Telescope (WXT) surveys $\sim$3600 deg^2 per exposure in the 0.5–4 keV band, while the Follow-up X-ray Telescope (FXT) provides rapid ($<$4 min slewing) deep imaging with a sensitivity of 10^{-13} erg cm^{-2} s^{-1} in 2 ks [6]. EP employs two trigger systems: (1) onboard triggers for bright events (e.g., GRBs) and (2) ground-processed triggers for fainter transients (e.g., FXTs), leveraging real-time data downlink through the Beidou system [7].

This article focuses on optical follow-up observations conducted by the BOOTES Global Network [8–10] for *EP* transients during its first year of operations. BOOTES comprises seven robotic stations equipped with 0.6 m Ritchey–Chretien telescopes, achieving a slewing speed of 100 deg/s and a pointing accuracy of $<5''$ [9]. Each telescope utilizes SDSS $u'g'r'i'$ and WFCAM/VISTA Z/Y filters, reaching limiting magnitudes of $m \approx 20.5$ in 300 s exposures [10]. In this work, we analyze the following:

- Time delays between the *EP* X-ray triggers and our optical observations.
- BOOTES's observational strategies and site-specific performance.
- Case studies of high-redshift GRBs (e.g., GRB 240315A at $z = 4.86$) and outstanding transients (e.g., EP240408a).

The synergy between *EP*'s rapid localization and the BOOTES network's robotic response has been demonstrated in multiple events (see Table 1), where BOOTES swiftly carried out optical follow-up observations to complement *EP*'s X-ray detections. This coordinated effort not only enabled rapid identification of potential afterglows but also paved the way for deeper spectroscopic studies using facilities like the GTC (Gran Telescopio CANARIAS) or VLT (Very Large Telescope), thereby greatly enhancing our understanding of these transient phenomena. Conversely, the absence of optical counterparts for EP240408a down to $r > 24$ mag challenges existing models of jetted TDEs [11]. These results highlight how optical follow-up not only complements X-ray data but also drives new theoretical inquiries.

Table 1. EP alert systems and BOOTES performance [6].

Parameter	Onboard Triggers	Ground Triggers
Energy Band	0.5–4 keV	0.5–4 keV
Brightness Threshold	$>10^{-9}$ erg cm^{-2} s^{-1}	$>10^{-11}$ erg cm^{-2} s^{-1}
Localization Accuracy	$\sim 1'$	$\sim 30''$

Section 2 details *EP*'s alert pipelines and BOOTES's observational protocols (Sections 2.1 and 2.2) as well as time response statistics and light curves (Section 2.3), while Section 3 discusses the astrophysical implications of key sources. Our findings establish a framework for optimizing transient follow-up in the multi-messenger era.

2. Methods

The transients analyzed in this paper were discovered by *Einstein Probe* (*EP*) between 19 February 2024 (the first source EP240219) and 26 February 2025. The data presented in this paper were compiled from various public sources, with a focus on optical follow-up observations conducted by the BOOTES network.

2.1. Data Sources

Our analysis focuses primarily on optical follow-up observations from ground-based facilities, particularly the BOOTES network. Key data sources include the following:

- The GCN (Gamma-Ray Coordinates Network) Circulars, which provide prompt notifications of EP detections, including source coordinates and discovery time (https://gcn.nasa.gov/circulars, accessed on 26 February 2025).
- The Astronomer's Telegram (ATel) reports, which contain follow-up observations and classification information from various teams (https://www.astronomerstelegram.org, accessed on 26 February 2025).
- Published papers focusing on specific *EP* sources, providing detailed multi-wavelength analysis and source characterization.

For each transient, we compiled key information such as the following:

- Discovery time and position.
- Multi-wavelength follow-up observations, with a focus on optical data from the BOOTES network.

2.2. BOOTES Network Follow-Up Observations

BOOTES (Burst Observer and Optical Transient Exploring System) is a global network of robotic telescopes designed for rapid response to transient alerts. Its strategic distribution across seven stations enables near-continuous monitoring and follow-up observations of transient astronomical events.

2.2.1. Telescope Network

The BOOTES network consists of seven stations (B1–B7) located across different continents, as shown in Table 2. Each station is equipped with a 0.6 m Ritchey–Chretien telescope, designed with fast-slewing capabilities to respond rapidly to transient alerts.

Table 2. BOOTES network sites location.

Site	Latitude	Longitude	Altitude (m)	Location
BOOTES-1	37°05′58.2″ N	6°44′14.89″ W	50	Mazagón, Spain
BOOTES-2	36°45′24.84″ N	4°02′33.83″ W	70	Algarrobo-Costa, Spain
BOOTES-3	45°02′22.92″ S	169°41′0.6″ E	360	Lauder, New Zealand
BOOTES-4	26°41′42.8″ N	100°01′48.24″ E	3200	Lijiang, China
BOOTES-5	31°02′39″ N	115°27′49″ W	2860	Baja California, Mexico
BOOTES-6	29°02′20″ S	26°24′13″ E	1383	Maselespoort, South Africa
BOOTES-7	22°57′09.8″ S	68°10′48.7″ W	2440	Atacama, Chile

2.2.2. Instrumentation and Observations

BOOTES telescopes are equipped with SDSS g', r', i' and WFCAM/VISTA Z and Y filters, along with Andor iXon X3 EMCCD cameras that provide a $10' \times 10'$ field of view. These telescopes can initiate observations within minutes of receiving an alert, ensuring timely multi-band photometry to capture the color evolution of transient sources. The limiting magnitudes vary based on telescope and exposure time, with BOOTES-5 reaching $m \approx 20.6$ mag in a 300 s exposure. The BOOTES network is also equipped with the low-resolution spectrograph COLORES [12] and has demonstrated its versatility in observing

diverse optical transients, including gamma-ray bursts and stellar flares. Its rapid slewing capability (<100 deg/s) ensures timely follow-up within critical observational windows.

Data reduction includes standard procedures such as bias subtraction, flat-fielding, and photometric calibration using Pan-STARRS reference stars [13]. Differential photometry is employed to analyze the brightness variations over time.

2.2.3. Response Times and Observational Strategy

The response time for BOOTES observations varies depending on the alert type. Onboard triggers for the brightest transients typically result in faster follow-up observations, while ground-based processed triggers for fainter events may have longer delays. For instance, Stellar flares typically exhibit rapid variability with durations of 1–2 h at most, as evidenced by the multi-wavelength observations of the DG CVn superflare [14]. Monitoring the delay between transient onset and the first observation is crucial for understanding the transient's early optical behavior.

2.2.4. Spectroscopic Follow-Up with 10.4 m GTC

Spectroscopic observations with the 10.4 m GTC telescope (+OSIRIS spectrograph) constitute a pivotal component of our multi-wavelength follow-up campaign. While the BOOTES network provides rapid optical imaging and initial photometric characterization, the high-resolution spectrum obtained here allows for a precise redshift determination and a thorough examination of the host galaxy's environment. These spectroscopic data enable us to investigate the physical conditions in the host and along the line of sight, offering critical insights into the interstellar and intergalactic media. Such information is essential not only for confirming the nature of the transient event but also for refining theoretical models of its progenitor system. Among the various sources we observed, the transient EP250215a is of particular interest. As an example, we show in Figure 1 the two-dimensional spectrum, which reveals a pronounced spectral break at ∼7100 Å, attributed to Lyα absorption.

In summary, the integration of fast-response imaging and detailed spectroscopic analysis exemplifies the comprehensive approach needed to unravel the complexities of these transient phenomena.

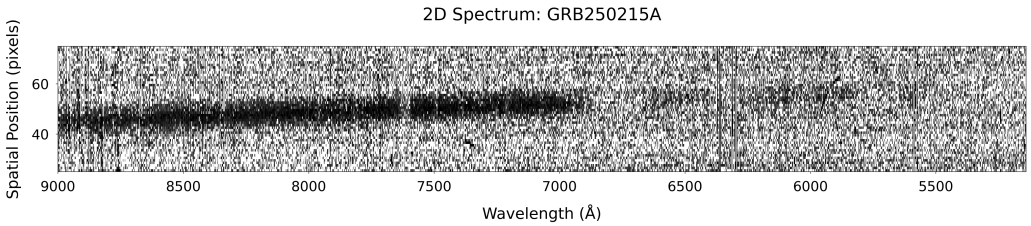

Figure 1. Two-dimensional spectrum of EP250215a obtained with GTC/OSIRIS. The red continuum remains smooth up to ∼7100 Å, beyond which a pronounced spectral break appears. This feature is attributed to Lyα absorption in the host galaxy's interstellar medium (ISM), while the blueward region is characterized by a Lyα forest produced by HI absorption from intervening intergalactic medium (IGM) clouds along the line of sight.

2.3. BOOTES Responsiveness

The BOOTES telescope network excels at rapid follow-up of astronomical transients, delivering near-real-time optical observations. Figure 2 breaks down, for each EP trigger, the interval from trigger to formal report ("Trigger → Report") and the ensuing BOOTES observation. Remarkably, in 53 of 113 cases (46.9%), BOOTES began observing before the formal report—i.e., negative tracking delays. To achieve millisecond-level ingestion and parsing of EP alerts, BOOTES relies on the GCN Kafka service (built on Apache

Kafka [15]). Kafka's high throughput allows the network to autonomously schedule observations even before GCN Circulars are issued, underpinning the "negative latency" measurements in Figure 2 and enabling capture of the earliest optical light curves. Figure 3 illustrates the response time distribution of the BOOTES network; fifteen logarithmically spaced bins were used to generate a normalized histogram of BOOTES response delays (in hours) on a logarithmic axis, highlighting the skewness of the distribution, demonstrating its exceptional capability for rapid follow-up observations of transient events, with the majority of observations commencing within the critical first hours after detection.

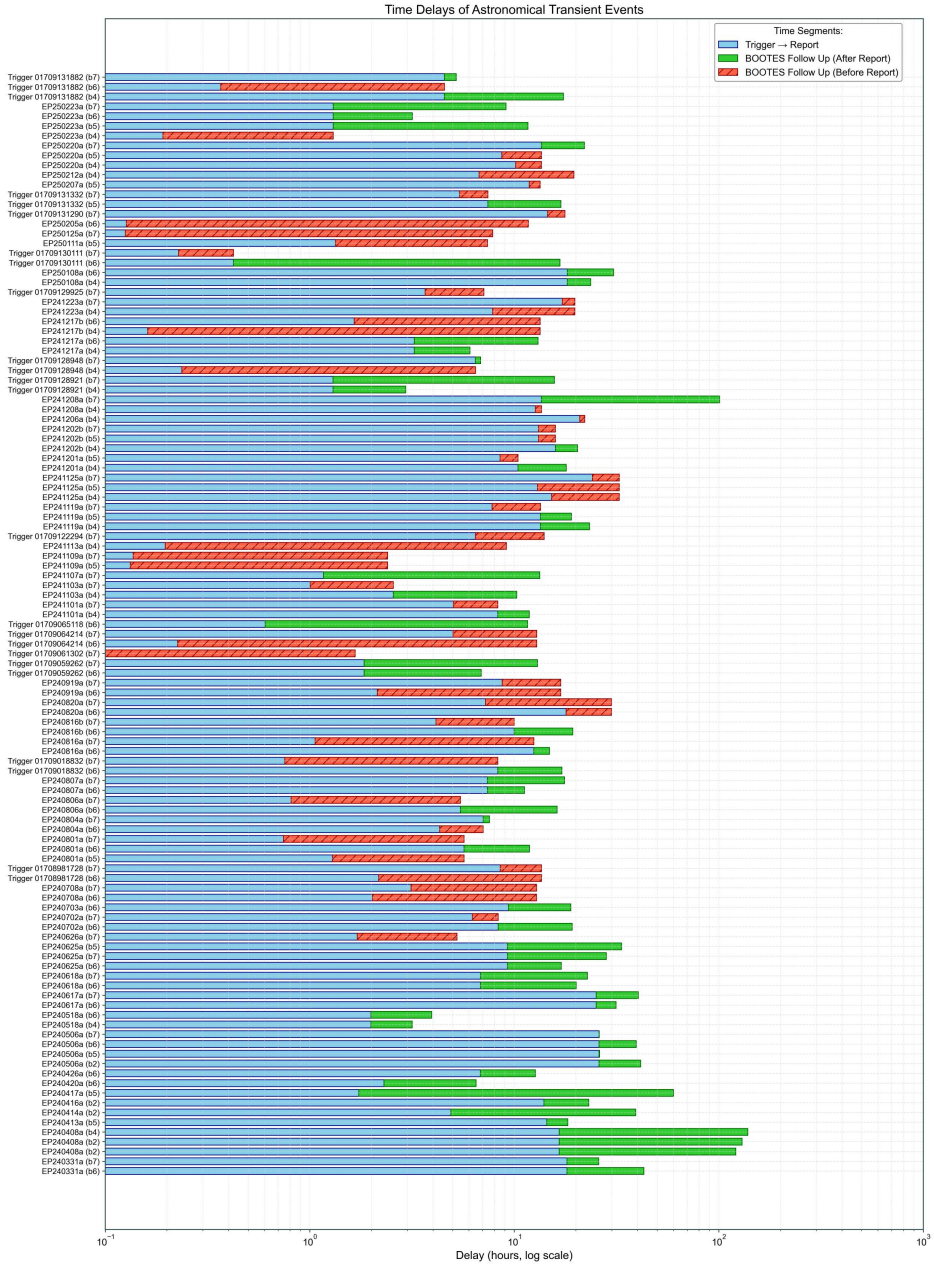

Figure 2. Time delays of BOOTES telescope network follow-up observations for *EP* transient sources, plotted on a logarithmic time axis (hours). Each horizontal bar is composed of up to three segments: (1) **Trigger → Report** (blue), showing the elapsed time from the EP trigger to the formal report; (2) **BOOTES Follow-Up (After Report)** (green), representing observations initiated after the report; (3) **BOOTES Follow-Up (Before Report)** (red), indicating negative tracking delays when BOOTES began observing prior to the report. Bars are offset from the origin by a small constant (left = 1×10^{-4}) to ensure visibility on the log scale. This chart highlights BOOTES's rapid-response capability across a wide dynamic range of follow-up latencies.

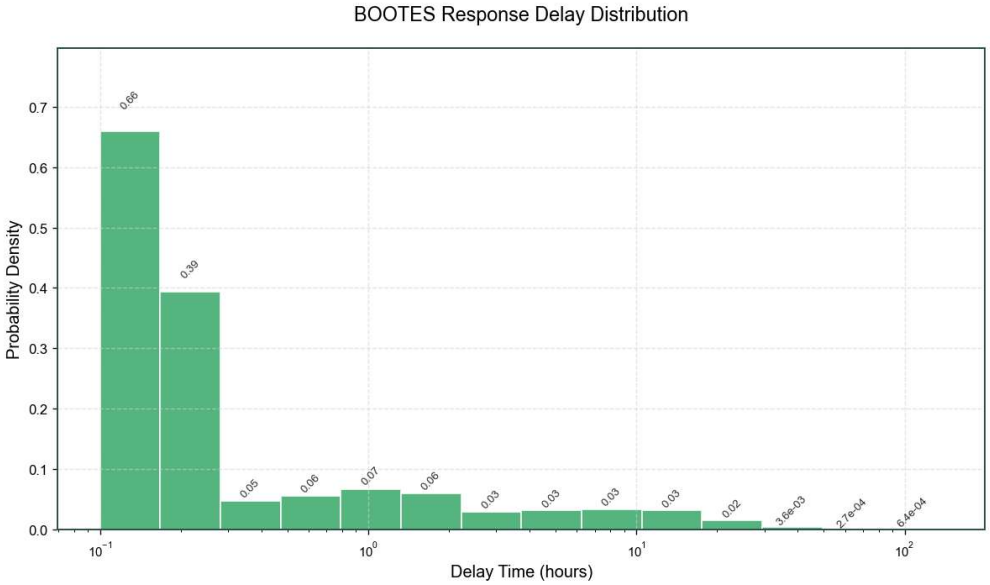

Figure 3. Distribution of BOOTES response delays to astrophysical transients initially detected by the EP telescopes. Despite the challenging slew and setup, BOOTES achieves follow-up within 1 h for 13.3% of triggers and within 3 h for 22.1% of triggers, capturing the crucial early-time emission before most observations begin.

Figure 4 shows the earliest optical detections and upper limits for *EP* sources observed by the BOOTES telescope network. The heterogeneous distribution of data points reflects the varying sensitivity and response times of the BOOTES telescopes. For example, the repeated observations of EP240426a by BOOTES-4 and BOOTES-6 demonstrate the network's capability to track transient evolution across multiple instruments.

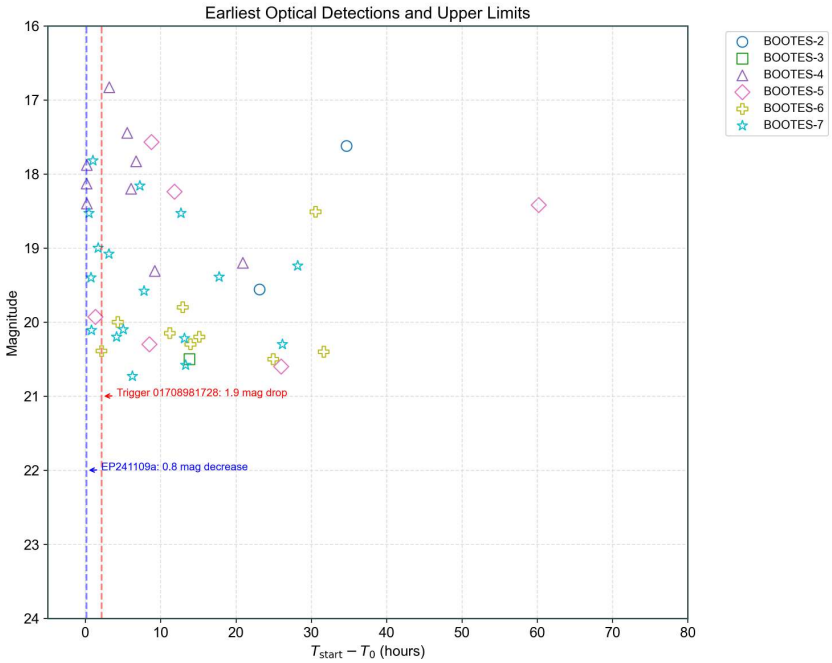

Figure 4. The earliest optical detections and upper limits for transients observed by the BOOTES telescope network. Magnitude values (or upper limits) are plotted against the time difference $T_{\text{start}} - T_0$ (hours), where T_0 is the initial trigger time. Data points are categorized by the BOOTES telescope identifier (BOOTES-2 to BOOTES-7), with empty markers indicating upper limits. Vertical dashed lines highlight special cases: a rapid brightness drop of 1.9 mag (red) and a 0.8 mag decrease (blue). The horizontal axis spans -5 to 80 h, and magnitudes range from 16 to 24.

BOOTES Network Observations of Multiple Sources

BOOTES network telescopes routinely conduct follow-up observations for *EP*-detected transients, providing detailed optical monitoring. Figure 5 shows selected sources observed across multiple epochs, demonstrating the BOOTES network's capability to track the temporal evolution of transients.

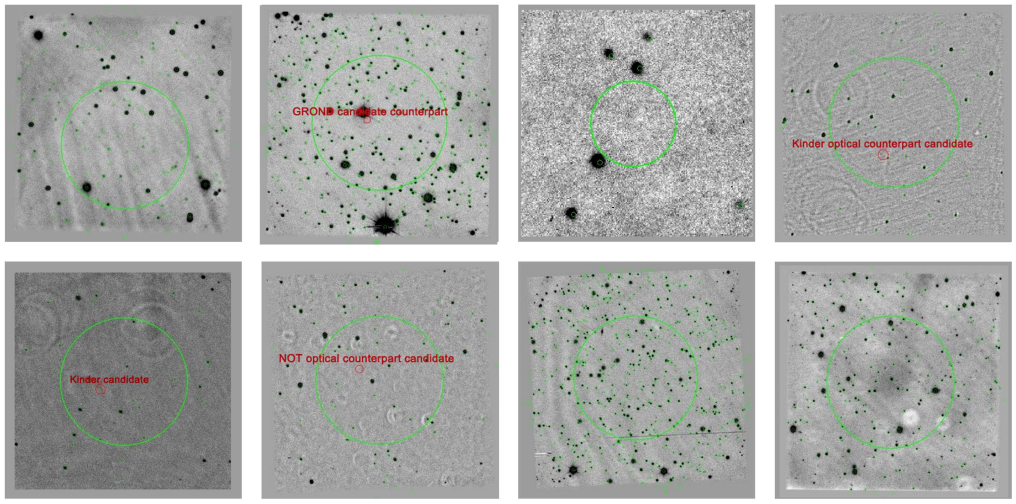

Figure 5. Some of the *EP* transients that were followed up on by the BOOTES network. The sources are arranged from left to right, top to bottom: EP240315a, EP240404a, EP240413a, EP240414a, EP240416a, EP240420a, EP240426a, and EP240506a. The green circles in the image denote sources detected by the telescope's automated source extraction algorithm. However, not all of these correspond to confirmed optical counterparts of the EP X-ray transient sources; some may be unrelated background objects or noise.

Optical light curves can be also provided automatically. As an example, the optical light curves of EP250110a, a flare star observed on 10 January 2025, using BOOTES-6 and BOOTES-7, are shown in Figure 6. These observations highlight significant brightness and color variations, with the *z*-band consistently showing brighter magnitudes compared to the *r*-band, suggesting significant spectral evolution, as seen in most active star flares [16].

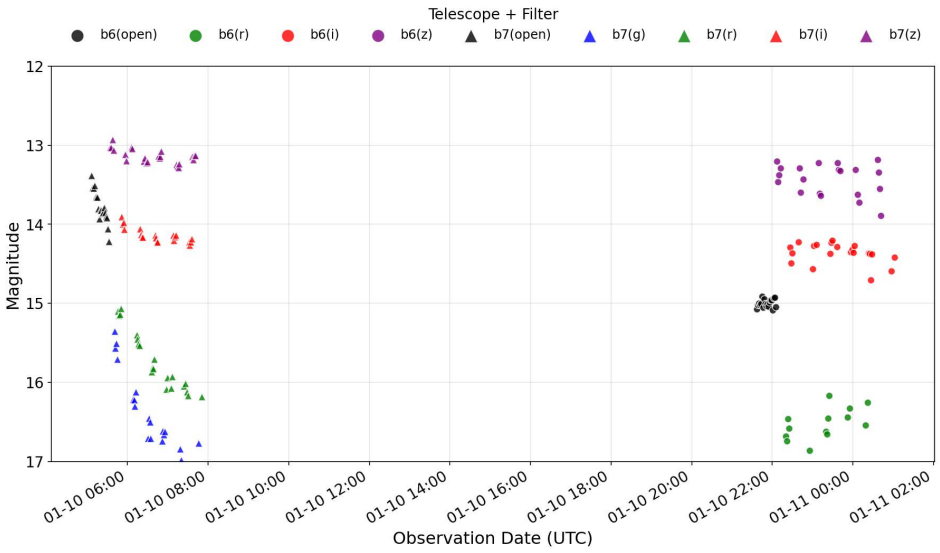

Figure 6. Filter-specific light curves of RX J0429.3-3124 obtained from BOOTES-6 (B6) and BOOTES-7 (B7) observations. Different filters are represented by distinct colors and symbols as indicated in the legend. Open symbols denote observations under suboptimal atmospheric conditions.

By focusing on the optical data and emphasizing response times, this section underscores BOOTES's role in providing rapid and high-quality follow-up observations that complement *EP*'s X-ray detections.

3. Overview of *EP* X-Ray Transients During the First Year

The spatial distribution of all *EP* transients detected during the first year of operation (from 19 February 2024 to 26 February 2025) is presented in Figure 7. A total of 128 transients were identified, with Fast X-ray Transients (FXTs) being the most numerous events (amounting to 52), followed by Gamma-Ray Bursts (GRBs) with 30 events, Stellar Flares with 28 events (bearing in mind that a very significant number remain unreported), Known Sources/Unclassified (14 events), and Optical Transients (4 events). The distribution exhibits a relatively isotropic pattern across the sky, with sources detected at all declinations. However, a slight deficit is observed near the Galactic plane, likely due to absorption effects and source confusion in these densely populated regions. This highlights the challenges of detecting transients in crowded fields, despite *EP*/WXT's wide field of view and sensitivity.

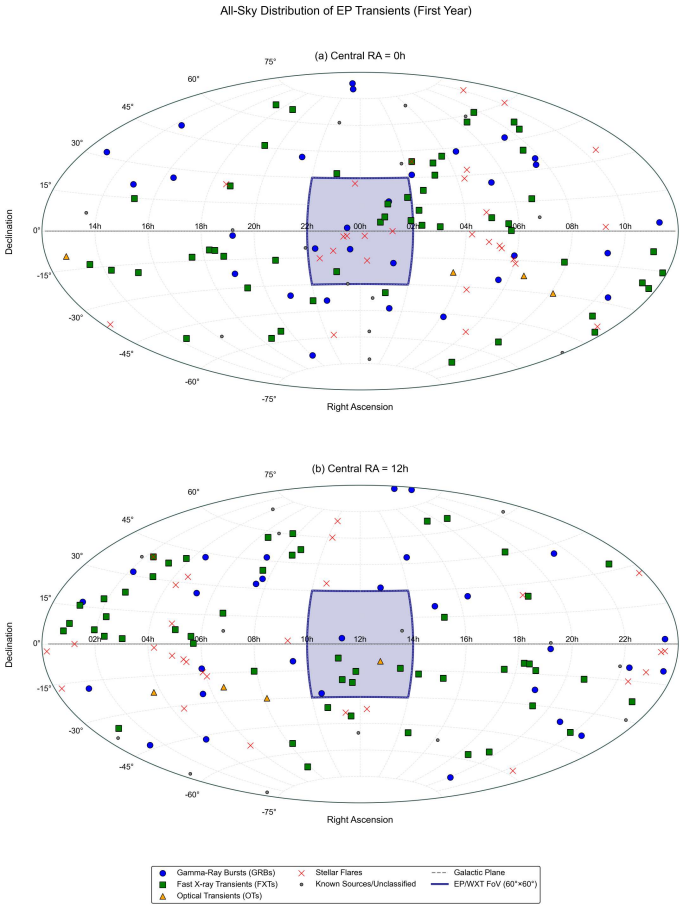

Figure 7. All-sky distribution of *EP* transients detected during the first year of operations, displayed in dual Aitoff projections with different coordinate centering. (**a**) Galactic distribution centered at RA = 0 h (vernal equinox) and (**b**) RA = 12 h (autumnal Equinox), both in J2000 equatorial coordinates. Source classes are differentiated by distinct markers: Gamma-Ray Bursts (blue circles), Fast X-ray Transients (green squares), Optical Transients (orange triangles), Stellar Flares (red crosses), and Known Sources/Unclassified (gray dots). The dashed black line traces the Galactic plane, while the blue shaded region demarcates the EP/WXT's instantaneous 60° × 60° field of view. This dual projection demonstrates complete celestial coverage and reveals longitudinal variations in transient distributions.

3.1. Source Classification

To systematically categorize the X-ray transients detected by *EP*, we classify each source into a primary category based on its dominant characteristics while noting any secondary classifications where applicable. The classification criteria are as follows:

- **Gamma-Ray Bursts (GRBs):**
  - Identified based on high-energy X-ray/gamma-ray emissions.
  - Typically exhibit short (<2 s) or long ($\gtrsim 2$ s) durations with rapid flux variability [17].
  - If associated with a known GRB event (e.g., detected by *Fermi*-GBM or *Swift*), they are classified as GRBs.
  - Sources with possible GRB-like properties but lacking definitive confirmation are marked as "Likely GRB".
- **Fast X-ray Transients (FXTs):**
  - Short-lived (typical time scale range of seconds to kiloseconds) X-ray flares without clear GRB signatures [18].
  - Exhibit sudden onset and rapid decay in flux.
  - May lack a known gamma-ray counterpart but show variability consistent with X-ray transients.
  - If an FXT also has multi-wavelength detections, it is marked with additional secondary classifications.
- **Optical Transients (OTs):**
  - Transients with detected optical counterparts, either from follow-up observations or archival surveys.
  - Includes events such as Fast Blue Optical Transients (FBOTs) and optical afterglow candidates of GRBs.
  - If an optical transient is associated with a confirmed astrophysical event (e.g., a supernova), this is noted in the classification.
- **Stellar Flares (M-dwarf Flares):**
  - X-ray events associated with active low-mass stars (e.g., M-dwarfs).
  - Identified based on position coincidence with known stellar objects (e.g., *Gaia* DR3 sources).
  - Typically exhibit high-energy flaring activity over timescales of seconds to minutes.
- **Known Sources/Unclassified:**
  - Transients that do not fit neatly into any of the above categories.
  - May include weak X-ray sources, events with insufficient data for robust classification, or candidates for future multi-wavelength follow-up.
  - X-ray activity from cataloged astrophysical objects such as cataclysmic variables (CVs), high-mass X-ray binaries (HMXBs) or active galactic nuclei (AGNs).

Each transient is assigned to a single primary category based on the dominant observed characteristics, with secondary classifications given in the "Notes" column, where applicable. This approach ensures that sources are not double-counted in statistical analyses while preserving additional classification context.

Rationale for Using First Observation Data: The data presented in the "X-ray properties" column of Table 3 are based solely on the initial observations made by the *EP*/FXT. This decision is motivated by the need for a uniform and consistent basis for classifying and comparing X-ray transients. The initial observation allows for determining the fundamental physical parameters (e.g., duration, peak flux, photon index) at the time of detection, which are crucial for establishing the primary characteristics of each event. Although follow-up

observations provide valuable insights into the temporal evolution and multi-wavelength behavior of the transients, incorporating these later data in the same column could lead to confusion by mixing the initial detection with subsequent changes. Instead, any supplementary information from follow-up observations is discussed in the following section (or in the accompanying notes).

Table 3. Classification of *EP* sources based on their nature and multi-wavelength observations.

Name	RA (deg)	Dec (deg)	X-Ray Properties	Notes
Gamma-Ray Bursts (GRBs)				
EPW20240219aa	80.016	25.541	Fast rise to $F_{\rm peak} \sim 5 \times 10^{-9}$ erg s^{-1} cm^{-2} (0.5–4.0 keV) in ∼10 s, decaying to background (4×10^{-11} erg s^{-1} cm^{-2}) in ∼200 s. Spectrum: absorbed power-law with $\Gamma = 2.0^{+0.9}_{-0.8}$, $N_H = 8.6^{+0.5}_{-0.4} \times 10^{21}$ cm^{-2}. $F_{\rm unabs} = 6.9^{+5.6}_{-2.1} \times 10^{-10}$ erg s^{-1} cm^{-2}	A weak, untriggered gamma-ray counterpart detected
EP240315a	141.644	−9.547	Duration: ∼1600 s, $F_{\rm peak}$: $\sim 3 \times 10^{-9}$ erg s^{-1} cm^{-2}, $N_H = (1.5^{+1.0}_{-0.9}) \times 10^{21}$ cm^{-2}, Γ: $1.7^{+0.4}_{-0.4}$, $F_{\rm unabs}$: $(5.3^{+1.0}_{-0.7}) \times 10^{-10}$ erg s^{-1} cm^{-2}	Mainly classified as GRBs, with secondary characteristics of FXTs and OTs (z = 4.859)
LXT240402A	245.451	25.763	$N_H = 4.3 \times 10^{20}$ cm^{-2}, $\Gamma = 1.7^{+0.1}_{-0.1}$, F (0.5–10 keV band): $7.8^{+0.8}_{-0.8} \times 10^{-13}$ erg s^{-1} cm^{-2}	Long GRB, associated with GRB 240402B, detected in 0.5–4 keV soft X-ray band, with FXT and OT secondary characteristics
EP240617a	285.030	−22.561	$F_{\rm peak,unabs}$: $\sim (1.4 \pm 0.1) \times 10^{-8}$ erg s^{-1} cm^{-2}, $\Gamma = 1.1 \pm 0.1$, $N_H = 1.7 \times 10^{21}$ cm^{-2}, $F_{\rm unabs}$: $(3.5 \pm 0.3) \times 10^{-9}$ erg s^{-1} cm^{-2}	X-ray-rich GRB, weak gamma-ray counterpart in Fermi/GBM data, likely GRB secondary classification
GRB240627B	215.25	48.52	1st Exposure: 586 s, Upper limit: 4.43×10^{-11} erg s^{-1} cm^{-2}; 2nd Exposure: 1233 s, Upper limit: 2.90×10^{-11} erg s^{-1} cm^{-2}	GRBs detected by SVOM: X-ray Upper Limits from EP-WXT
GRB240629A	314.4	−35.7	1st Exposure: 6429 s, Upper limit: 1.18×10^{-11} erg s^{-1} cm^{-2}; 2nd Exposure: 54,140 s, Upper limit: 3.93×10^{-12} erg s^{-1} cm^{-2}	GRBs detected by SVOM: X-ray Upper Limits from EP-WXT
GRB240713A	352.59	1.88	A total of 13.3 h after the detection of SVOM/ECLAIRs, the exposure time is about 6.8 ks; 10 X-ray sources were found within the SVOM/ECLAIRs localization error box	X-ray follow-up observation with EP-FXT
EP240802a	287.8070	−2.3125	Dur. > 500 s, lightcurve from WXT shows three sequentially weakened peaks, $N_H = 2.5^{+2.0}_{-1.8} \times 10^{21}$ cm^{-2}, $\Gamma = 0.94^{+0.59}_{-0.56}$, and $F_{\rm unabs,average} = 1.7^{+0.4}_{-0.3} \times 10^{-9}$ erg s^{-1} cm^{-2}. For the average FXT spectrum in the 0.5–10 keV band, $N_H = 4.8^{+1.4}_{-1.2} \times 10^{21}$ cm^{-2}, $\Gamma = 1.89^{+0.33}_{-0.31}$, $F_{\rm unabs,average} = 1.3^{+0.2}_{-0.1} \times 10^{-12}$ erg s^{-1} cm^{-2}	Associated with long GRB 240802A
EP240804a	337.644	−39.121	For the WXT observed transient: Dur. > 100 s, $N_H = 1.1^{-1.0}_{+37.0} \times 10^{20}$ cm^{-2}, $\Gamma = 0.7^{-0.4}_{+1.2}$, $F_{\rm unabs,average} = 6.1^{-1.6}_{+2.6} \times 10^{-10}$ erg s^{-1} cm^{-2} (0.5–4 keV) For the FXT: The light curve shows significant variability. For the 0.5–10 keV spectrum, $N_H = 2.8^{+2.7}_{-2.7} \times 10^{20}$ cm^{-2}, $\Gamma = 1.6^{+0.1}_{-0.1}$, $F_{\rm unabs,average} = 2.2^{+0.1}_{-0.1} \times 10^{-11}$ erg s^{-1} cm^{-2}	Associated with GRB 240804B; optical candidate with large deviation detected
EP240807a	300.970	−68.777	Dur. ∼ 70 s, $F_{\rm peak}$: $\sim 1 \times 10^{-8}$ erg s^{-1} cm^{-2}, $\Gamma = 0.9^{+1.7}_{-0.8}$, $N_H = 1.1^{+1.6}_{-1.1} \times 10^{21}$ cm^{-2}, $F_{\rm unabs}$: $1.7^{+0.7}_{-0.6} \times 10^{-10}$ erg s^{-1} cm^{-2}	Associated with GRB 240807A; X-ray afterglow confirmed by EP-FXT

Table 3. *Cont.*

Name	RA (deg)	Dec (deg)	X-Ray Properties	Notes
GRB240821A	354.23	−10.18	source #1 (RA = 354.2701 deg, DEC = −10.1911 deg): 1st epoch: TGRB-Tstart = 8.8 h, Exposure = 5.0 ks, Estimated Flux = $(1.1 \pm 0.2) \times 10^{-13}$ erg s^{-1} cm^{-2}; 2nd epoch: TGRB-Tstart = 15.2 h, Exposure = 8.0 ks, Estimated Flux = $(5.9 \pm 1.3) \times 10^{-14}$ erg s^{-1} cm^{-2}; 3rd epoch: TGRB-Tstart = 111.4 h, Exposure = 8.4 ks, Estimated Flux < 1.5×10^{-14} erg s^{-1} cm^{-2} source #2 (RA = 354.1516 deg, DEC = −10.0504 deg): 1st epoch: TGRB-Tstart = 8.8 h, Exposure = 5.0 ks, Estimated Flux = $(6.0 \pm 1.3) \times 10^{-14}$ erg s^{-1} cm^{-2}; 2nd epoch: TGRB-Tstart = 15.2 h, Exposure = 8.0 ks, Estimated Flux = $(3.5 \pm 1.0) \times 10^{-14}$ erg s^{-1} cm^{-2}; 3rd epoch: TGRB-Tstart = 111.4 h, Exposure = 8.4 ks, Estimated Flux < 3.4×10^{-14} erg s^{-1} cm^{-2}	Detected as a short-duration GRB by multiple instruments, with X-ray afterglow
EP240913a	16.681	16.750	At ∼T0 + 180 s, the light-curve has a fast pulse (Dur. ∼50 s) followed by weak emission up to 1100 s. $F_{\rm peak}$: $\sim 2 \times 10^{-9}$ erg s^{-1} cm^{-2}, $\Gamma = 0.5^{+0.6}_{-0.6}$, $N_H = 5.1 \times 10^{20}$ cm^{-2} (fixed), $F_{\rm unabs}$: $1.1^{+0.5}_{-0.4} \times 10^{-10}$ erg s^{-1} cm^{-2}	Short gamma-ray burst, consistent in time and space with X-ray transient
EP240919a	334.2797	−9.7362	Dur. > 400 s, $N_H = 5.4 \times 10^{20}$ cm^{-2}, $\Gamma = 1.3^{+0.3}_{-0.3}$, $F_{\rm absorbed,average} = 7.0^{+1.8}_{-1.5} \times 10^{-10}$ erg s^{-1} cm^{-2} (0.5–4 keV)	Associated with long GRB 240919A; radio counterpart candidate detected at 9 GHz
EP240930a	319.899	41.303	$\Gamma = 0.79^{+0.24}_{-0.25}$, $N_H = 3.29 \times 10^{21}$ cm^{-2} (fixed), $F_{\rm unabs}$: $3.8^{+0.5}_{-0.5} \times 10^{-9}$ erg s^{-1} cm^{-2}	Consistent with long GRB 240930B in time and space, X-ray afterglow characteristics support GRB classification, also has FXT characteristic in initial stage
GRB241001A	20.55276	−43.47506	The source faded by an order of magnitude to $F_X = (5.1 \pm 1.2) \times 10^{-14}$ erg cm^{-2} s^{-1} in the 0.3–10 keV band. Confirmed: Swift/XRT source #2 is the afterglow of GRB 241001A	The optical counterpart was detected, qualifies as an X-Ray Flash (XRF), z = 0.573
GRB241018A	67.9992	43.0200	$N_H = 9.5^{+6.9}_{-5.7} \times 10^{21}$ cm^{-2}, $\Gamma = 2.5^{+1.2}_{-1.1}$, Observed flux (0.5–10.0 keV): $1.8^{+1.6}_{-0.7} \times 10^{-13}$ erg s^{-1} cm^{-2}	Detected by multiple gamma-ray detectors, X-ray afterglow consistent with GRB characteristics
EP241025a	333.6408	83.5772	Trigger flux (0.5–4 keV, assumed $\Gamma = 2$ absorbed power-law): $\sim 2 \times 10^{-10}$ erg s^{-1} cm^{-2}, Source flux: $\sim 5 \times 10^{-11}$ erg s^{-1} cm^{-2}	Long GRB, the optical counterpart was detected, z = 4.20
EP241030a	343.013	80.449	$\Gamma = 2.5^{+0.8}_{-0.7}$, $N_H = 1.8 \times 10^{21}$ cm^{-2} (fixed), $F_{\rm unabs}$: $7.5^{+3.0}_{-2.4} \times 10^{-11}$ erg s^{-1} cm^{-2}	GRB 241030A X-ray Afterglow
EP241104a	32.574	31.555	Dur. $\sim 400\,s$, $F_{\rm peak}$: $\sim 5.0 \times 10^{-10}$ erg s^{-1} cm^{-2} (0.5–4 keV), $\Gamma = 1.3^{+0.8}_{-0.7}$, $N_H = 7.8 \times 10^{20}$ cm^{-2} (fixed), $F_{\rm unabs}$: $2.0^{+1.0}_{-1.1} \times 10^{-10}$ erg s^{-1} cm^{-2}	Associated with known GRB 241104A
GRB241105A	61.9	−46.7	For the two observations, the first one has an exposure time of 2894 s, $T_{mid} - T_0$ of 22.0 h, and a flux in the 0.5–10 keV band of $(1.51 \pm 0.31) \times 10^{-13}$ erg s^{-1} cm^{-2}; the second one has an exposure time of 7966 s, $T_{mid} - T_0$ of 38.0 h, and a flux in the 0.5–10 keV band of $(3.79 \pm 0.50) \times 10^{-14}$ erg s^{-1} cm^{-2}	Known GRB event, multi-band observations support short-burst with extended radiation characteristics
EP241113b	110.233	46.800	$\Gamma = 1.5^{+0.7}_{-0.7}$, $N_H = 2.7 \times 10^{21}$ cm^{-2} (with an uncertainty of $\pm 1.8 \times 10^{21}$ cm^{-2}), $F_{\rm unabs}$: $1.5^{+0.4}_{-0.4} \times 10^{-9}$ erg s^{-1} cm^{-2}, Dur. of lightcurve from WXT = 100 s	Associated with known GRB event, multi-band observations support the classification
EP241115a	19.416	−17.954	$\Gamma = 1.50^{+0.38}_{-0.38}$, $N_H = 1.6 \times 10^{20}$ cm^{-2} (fixed), $F_{\rm unabs,0.3-10keV}$: $2.1^{+0.9}_{-0.5} \times 10^{-12}$ erg s^{-1} cm^{-2}	Associated with GRB 241115D
EP241213a	116.182	35.271	$\Gamma = 2.2^{+1.4}_{-1.4}$, $N_H = 5.9 \times 10^{21}$ cm^{-2} (with an uncertainty of $\pm 4.8 \times 10^{21}$ cm^{-2}), $F_{\rm unabs}$: 5.2×10^{-11} erg s^{-1} cm^{-2}	Associated with long GRB 241213A

Table 3. *Cont.*

Name	RA (deg)	Dec (deg)	X-Ray Properties	Notes
EP241217b	84.167	−25.281	WXT: - Light curve: 2 pulses. 1st from 10–620 s (2 short pulses at 150 s and 260 s, slewing 53–134 s), 2nd from 1000–1500 s. - Spectrum (134–2000 s after GRB trigger): Absorbed power-law, $N_{H,MW} = 1.79 \times 10^{20}$ cm^{-2} (fixed), $z = 1.195$, $N_{H,int} = 1.42^{+0.51}_{-0.46} \times 10^{22}$ cm^{-2}, $\Gamma = 1.57^{+0.22}_{-0.21}$, $F_{\rm unabs,0.5–4keV} = (1.19 \pm 0.10) \times 10^{-9}$ erg s^{-1} cm^{-2} FXT: - Spectrum (134–7800 s after GRB trigger, annular region): Same model as WXT. $N_{H,int} = 0.85 \pm 0.06 \times 10^{22}$ cm^{-2}, $\Gamma = 1.58 \pm 0.04$, $F_{\rm unabs,0.5–10keV} = 1.1 \times 10^{-9}$ erg s^{-1} cm^{-2}	Associated with GRB 241217A, z = 1.879
GRB241229A	192.893	31.857	EPF_J125139.4 + 315,311: R.A. = 192.9133 deg, DEC = 31.8867 deg, Sep. = 2.06 arcmin, $F = 6.82 \times 10^{-14}$ erg s^{-1} cm^{-2} EPF_J125129.3 + 314,453 : R.A. = 192.8715 deg, DEC = 31.7484 deg, Sep. = 6.61 arcmin, $F = 7.73 \times 10^{-13}$ erg s^{-1} cm^{-2} EPF_J125101.6 + 315,007: R.A. = 192.7572 deg, DEC = 31.8356 deg, Sep. = 7.04 arcmin, $F = 9.25 \times 10^{-14}$ erg s^{-1} cm^{-2}	Long GRB, EP-FXT detected afterglow candidates
EP250109a	88.806	−12.500	WXT (EP250109a, trigger at 2025-01-09T06:17:58 UTC): - Peak: ∼60 s post-trigger, $F_{\rm peak,0.5–4keV} \approx 2.5 \times 10^{-9}$ erg s^{-1} cm^{-2} - Decay: To background within 200 s post-trigger - Spectrum: Absorbed power law, $\Gamma = 2.9 \pm 1.0$, $N_{H,Gal} = 3.04 \times 10^{21}$ cm^{-2} (fixed), $z = 0$, $N_{H,int} = 5.0^{+0.4}_{-0.3} \times 10^{21}$ cm^{-2}, $F_{\rm unabs,0.5–4keV} = 2.5^{+4.6}_{-1.2} \times 10^{-9}$ erg s^{-1} cm^{-2} FXT (Obs. start: 2025-01-09T08:06:40 UTC, ∼1.8 h post-trigger, $t_{exp} \approx 4.2$ ks): - Spectrum: Absorbed power-law, $\Gamma = 1.9^{+1.9}_{-0.7}$, $N_{H,Gal} = 3.04 \times 10^{21}$ cm^{-2} (fixed), $z = 0$, $N_{H,int} \approx 3 \times 10^{20}$ cm^{-2}, $F_{\rm unabs,0.5–4keV} = 4.9^{+2.0}_{-1.2} \times 10^{-13}$ erg s^{-1} cm^{-2}	Associated with GRB 250109A, multi-band observations support the classification
GRB250127A	169.6284	3.3508	$\Gamma = 1.79^{+0.92}_{-0.92}$, $N_{H,Gal} = 4.52 \times 10^{20}$ cm^{-2} (fixed), $F_{\rm unabs,0.5–10keV}$: $1.30^{+1.44}_{-0.68} \times 10^{-13}$ erg s^{-1} cm^{-2}	Long GRB event
EP250205a	113.522	32.363	WXT (0.5–4.0 keV): - Absorbed power-law, $N_{H,Gal} = 4.4 \times 10^{20}$ cm^{-2} (fixed), $z = 3.55$ - $N_{H,int} = 6.5^{+9.8}_{-6.5} \times 10^{22}$ cm^{-2}, $\Gamma = 2.5^{+1.7}_{-1.2}$, $F_{\rm unabs,0.5–4keV} = 4.2^{+1.1}_{-1.1} \times 10^{-10}$ erg s^{-1} cm^{-2} EP-FXT (average 0.5–10 keV): - Absorbed power-law, $N_{H,Gal} = 4.4 \times 10^{20}$ cm^{-2} (fixed) - $\Gamma = 2.82^{+0.06}_{-0.04}$, $F_{\rm unabs,0.5–10keV} = 3.65^{+0.07}_{-0.09} \times 10^{-11}$ erg s^{-1} cm^{-2}	Associated with GRB 250205A, optical counterpart was detected
EP250215a	156.3430	−27.7040	Duration = —, Peak flux = —	Associated with long GRB 250215A, optical counterpart was detected, z = 4.61
EP250226a	224.273	20.973	WXT detection: Dur. = 22 s, $F_{\rm peak,0.5–4\,keV} = 9.8 \times 10^{-9}$ erg s^{-1} cm^{-2} (trigger at 2025-02-26T06:34:54 UTC). FXT follow-up: First epoch (44 min post-trigger): $\Gamma = 2.07^{+0.06}_{-0.06}$, $N_{H,Gal} = 3.7 \times 10^{20}$ cm^{-2} (fixed), $F_{\rm unabs,0.5–10\,keV} = 2.89^{+0.08}_{-0.08} \times 10^{-11}$ erg s^{-1} cm^{-2} at R.A. = 224.2641°, Dec. = 20.9754° (10 arcsec error). Second epoch (11.9 h post-trigger): $F_{\rm unabs,0.5–10\,keV} = 1.83^{+0.18}_{-0.18} \times 10^{-12}$ erg s^{-1} cm^{-2}, indicating X-ray $L_{\rm jump} \sim 16\times$ decline	Associated with GRB 250226A, optical counterpart detected, z = 3.315

Table 3. *Cont.*

Name	RA (deg)	Dec (deg)	X-Ray Properties	Notes
Stellar Flares (M-dwarf flares)				
EP trigger ID 01708913080	336.13	−58.429	Spectrum Model: Two apec components, $T_1 = 0.89^{+0.05}_{-0.07}$ keV, $T_2 = 2.9 \pm 0.3$ keV, $F_{\mathrm{FXT,0.5–10keV}} = 3.0 \pm 0.1 \times 10^{-11}$ erg s^{-1} cm^{-2} (2 orders of magnitude higher than eROSITA flux) If associated with M star, $L_{\mathrm{peak}} = 7.6 \times 10^{29}$ erg s^{-1}	Associated with M-dwarf UPM J2224-5826, X-ray flux significantly higher than eROSITA historical value
EP trigger ID 01708981728	336.513	−15.302	Spectrum Model: Two absorbed apec components, $T_1 = 0.93 \pm 0.03$ keV, $T_2 = 4.1 \pm 0.2$ keV, $N_H = 9.0^{+0.7}_{-0.6} \times 10^{20}$ cm^{-2}, $F_{\mathrm{unabs,0.5–10keV}} = 3.6 \pm 0.3 \times 10^{-10}$ erg s^{-1} cm^{-2} If associated with high-proper-motion star, $L_{\mathrm{peak,0.5–10keV}} = 4.0 \times 10^{31}$ erg s^{-1}	Associated with high-proper-motion star LP 820-19, optical observation confirms significant brightness enhancement during flare
EP trigger ID 01709018832	2.562	−2.665	Spectrum Model: Two absorbed apec components, $T_1 = 1.03^{+0.08}_{-0.08}$ keV, $T_2 = 4.49^{+1.10}_{-0.76}$ keV, $N_H = 0$ (fixed) $F_{\mathrm{0.5–10keV}} = 6.51^{+0.55}_{-0.51} \times 10^{-12}$ erg s^{-1} cm^{-2} If source associated with star, $L_{\mathrm{peak}} = 4.1 \times 10^{31}$ erg s^{-1}	Associated with M-dwarf Gaia DR3 2445442335531658752, optical observation shows significant brightness change during flare
EP trigger ID 01709059262	278.807	24.588	The position of the FXT source is associated with the star 2MASS J18351416 + 2,435,115	Spectrum: Red continuum + strong Balmer, Ca II H&K, TiO emission lines, consistent with dMe star spectrum
EP trigger ID 01709061302	350.5437	−3.0283	The FXT source is associated with a K-type star, PM J23221-0301, at a distance of about 46 pc and located about 8 arcsec away from the FXT position	—
EP trigger ID 01709064214	352.558	−2.614	n M-type, high proper motion star 2MASS J23301129-0237227/2RXS J233013.0-023738, is at a distance of about 46 pc and located about 5.1 arcsec away from the position detected by FXT	The X-ray transient was also detected in the optical and confirm it originated from a flare star
EP trigger ID 01709065118	344.5674	−11.0724	The FXT source is associated with an M-type star, 1RXS J225817.2-110434, at a distance of about 32 pc and located about 5 arcsec away from the FXT position	Spectra: Red continuum + strong H Balmer, Ca II H&K, TiO emission lines, consistent with dMe star spectrum. Photometry: Trigger event associated with stellar flare
EP241109a	18.3599	0.0184	In GAIA DR3, a close star ($T_{\mathrm{eff}} \approx 3200$ K, $d \approx 71.83$ pc) lies within EP-FXT error circle of EP241109a	GAIA DR3 2534635509050352256: Brightness decreased by 0.8 mag (clear filter) in 40 min, confirming EP241109a as a stellar flare. Based on photometry and spectroscopy, EP241109a event is associated with this stellar flare
EP trigger ID 01709120856	4.023	−16.604	$F_{\mathrm{peak}} \approx 8 \times 10^{-11}$ erg s^{-1} cm^{-2}, $L_X \approx 3 \times 10^{30}$ erg s^{-1} (typical for M-type dwarf)	—
EP trigger ID 01709122294	64.628	28.458	Spectrum Model: Absorbed apec, $T = 3^{+5}_{-1}$ keV $F_{\mathrm{unabs,0.5–4keV}} = 3.7^{+1.3}_{-1.1} \times 10^{-11}$ erg s^{-1} cm^{-2} If the transient is associated with V410 Tau, $L_{\mathrm{0.5–4keV}} \approx 7.3 \times 10^{31}$ erg s^{-1}	Flare decay in observations: - In u and v bands: magnitudes decayed 0.24 and 0.11 in 7 h. - In g and r bands: no significant variations
EP trigger ID 01709128921	63.363	−1.648	Associated with a double or multiple star RX J0413.4-0139, $F_{\mathrm{peak}} \approx 2.0 \times 10^{-10}$ erg s^{-1} cm^{-2}, corresponding to $L_X \approx 1.7 \times 10^{31}$ erg s^{-1}	—
EP trigger ID 01709128948	79.405	−7.557	Associated with a young stellar object candidate ATO J079.4052-07.5576, $F_{\mathrm{0.5–10.0keV}} \approx (1.05 \pm 0.02) \times 10^{-10}$ erg s^{-1} cm^{-2}, corresponding to $L_X \approx (1.74 \pm 0.03) \times 10^{33}$ erg s^{-1}	—
EP trigger ID 01709129023	151.839	69.35	Associated with an eruptive variable UCAC4 797-019583, $F_{\mathrm{peak}} \approx 1.8 \times 10^{-10}$ erg s^{-1} cm^{-2}, corresponding to$L_X \approx 6 \times 10^{31}$ erg s^{-1}	—
EP trigger ID 01709129287	88.836	−14.381	Associated with a high proper motion star TYC 5360-423-1, $F_{\mathrm{0.5–10.0keV}} \approx 2 \times 10^{-11}$ erg s^{-1} cm^{-2}, corresponding to$L_X \approx 5 \times 10^{31}$ erg s^{-1}	—

Table 3. *Cont.*

Name	RA (deg)	Dec (deg)	X-Ray Properties	Notes
EP trigger ID 01709129925	90.609	−16.579	Associated with a high proper motion star 1RXS J060224.9-163451, $F_{\rm peak} \approx 1 \times 10^{-10}$ erg s^{-1} cm^{-2}, corresponding to$L_X \approx 2 \times 10^{31}$ erg s^{-1}	—
EP trigger ID 01709130111	67.339	−31.395	Associated with a low-mass star, RX J0429.3-3124, $F_{\rm peak} \approx 1.6 \times 10^{-10}$ erg s^{-1} cm^{-2}, corresponding to$L_X \approx 5.5 \times 10^{30}$ erg s^{-1}	—
EP trigger ID 01709131085	72.216	10.03	Associated with a high proper motion star RX J0448.7 + 1003, $F_{\rm peak} \approx 2.0 \times 10^{-10}$ erg s^{-1} cm^{-2}, $L_X \approx 7.1 \times 10^{30}$ erg s^{-1}	Photometry: - At 26.7 min, $B \approx 13.2$ mag. - Peaked at 43.6 min with $B \approx 12.9$ mag. - At 187 min, $B \approx 13.6$ mag. Conclusion: EP-WXT trigger event is associated with the stellar flare
EP trigger ID 01709131196	139.021	1.89	Associated with an M-type star RX J0916.1 + 0153, $L_{0.5-10\rm keV}^{\rm preliminary} \approx 5.4 \times 10^{29}$ erg s^{-1}	—
EP trigger ID 01709131290	88.148	−53.067	Associated with a star UCAC4 185-006985, $F_{\rm peak} \approx 1.9 \times 10^{-10}$ erg s^{-1} cm^{-2}, corresponding to $L_X \approx 5.5 \times 10^{31}$ erg s^{-1}	—
EP trigger ID 01709131332	184.462	−36.741	Associated with a high proper motion star UPM J1217-3644, $F_{\rm peak} \approx 1.2 \times 10^{-10}$ erg s^{-1} cm^{-2}, $L_X \approx 1.2 \times 10^{31}$ erg s^{-1}	—
The EP trigger 01709131347	158.298	34.176	Associated with a spectroscopic binary G 118-68, $F_{\rm peak} \approx 1.0 \times 10^{-10}$ erg s^{-1} cm^{-2}, corresponding to $L_X \approx 2.5 \times 10^{31}$ erg s^{-1}	—
EP250207a	356.902	27.027	Associated with low-mass star 2MASS J23473680 + 2,702,068, 0.5–4 keV single-apec fit - Spectrum fit: 0.5–4 keV spectrum fitted with a single apec model, $T = 3.1^{+5.9}_{-1.2}$ keV, no significant absorption. - Flux: $F_{0.5-4\rm keV} = 2.9^{+0.9}_{-0.7} \times 10^{-10}$ erg s^{-1} cm^{-2} 0.3–10 keV two-apec fit - Spectrum fit: 0.3–10 keV spectrum fitted with two apec components, $T_1 = 0.75^{+0.2}_{-0.3}$ keV, $T_2 = 2.6^{+1.3}_{-0.6}$ keV, no significant absorption. - Flux and luminosity: $F_{0.3-10\rm keV} = 9.2^{+1.1}_{-1.0} \times 10^{-12}$ erg s^{-1} cm^{-2}, $L_X \approx 5 \times 10^{29}$ erg s^{-1}	This high-proper-motion M9 dwarf brightened from $r = 19.8 \pm 0.1$ (Pan-STARRS) to $r = 16.9 \pm 0.1$. Gaia DR3 shows a proper motion of 315.33 ± 0.21 mas/yr and parallax of 46.76 ± 0.16 mas, suggesting it is a nearby star having a +3-mag flare
EP J0433.6+3255	68.4	32.917	Dur. $>$ 2000 s. The source is $\sim$ 30 arcsec from an ROSAT X-ray source (1RXS J043335.1 + 325,432), which is spatially consistent with a nearby M-type star (Gaia DR3 1720422723228817 92; Assoc.: M-type star). The separation between the star and 1RXS J043335.1 + 325,432 is 11 arcsec. The outburst may be associated with both the M-type star (Assoc.: M-type star) and the X-ray source (Assoc.: X-ray source). If confirmed, the X-ray $F_{\rm peak}$ would show a $\sim$100-fold increase compared to the ROSAT $F_{\rm peak}$ (2.2×10^{-13} erg s^{-1} cm^{-2}). The WXT spectrum is best fitted by an absorbed power-law with $\Gamma = 2.5^{+1.8}_{-1.7}$ and $N_H = 2.3 \times 10^{21}$ cm^{-2} (fixed). The corresponding $F_{\rm unabs}$ is $3.0^{+1.7}_{-1.3} \times 10^{-11}$ erg s^{-1} cm^{-2}. If associated with Gaia DR3 172042272322881792, the 0.5–4 keV luminosity $L_X \approx 6.4 \times 10^{30}$ erg s^{-1}	—
EP J0452.7-0541	73.176	−5.687	Source position matches 1eRASS J045241.6-054101 with $F_{\rm peak} = 3.0 \times 10^{-13}$ erg s^{-1} cm^{-2} (0.2–2.3 keV). Associated with Gaia DR3 3188422199717067648 (separation 1.4 arcsec; Assoc.: star). WXT spectrum: abs apec model with $T = 2.8^{+3.7}_{-1.0}$ keV, $N_H = 3.8 \times 10^{20}$ cm^{-2} (fixed). $F_{\rm unabs} = 4.3^{+1.4}_{-1.1} \times 10^{-11}$ erg s^{-1} cm^{-2} ($\sim$100$\times$ brighter than eROSITA). If associated, $L_X \approx 3.9 \times 10^{31}$ erg s^{-1} (0.5–4 keV)	—

Table 3. *Cont.*

Name	RA (deg)	Dec (deg)	X-Ray Properties	Notes
RX J0218.7+3854	34.6990	38.9136	FXT source spatially matches *Gaia* DR3 331926892386271872 (offset 3 arcsec; Assoc.: Gaia object). Spectrum (0.5–10 keV): absorbed power-law with $\Gamma = 2.6^{+0.2}_{-0.2}$, $N_H = 5.47 \times 10^{20}$ cm^{-2} (fixed). $F_{\rm unabs} = 4.9^{+0.5}_{-0.4} \times 10^{-13}$ erg s^{-1} cm^{-2}, consistent with historical *ROSAT* flux. Spatial correlation with EP241206a suggests the WXT detection may represent an X-ray outburst from RX J0218.7 + 3854	—
EP241212a	153.817	60.068	Faint X-ray source 1WGA J1015.3 + 6004/Gaia DR3 1048515045825830144 (R.A. = 153.83607, Dec. = +60.07485) at $d \approx 107$ pc, offset 42 arcsec from WXT position. No significant variability. WXT spectrum: absorbed power-law with $\Gamma = 2.7^{+1.0}_{-1.0}$, $N_H = 3.8^{+2.7}_{-2.7} \times 10^{21}$ cm^{-2}. Absorbed 0.5–4 keV flux: $1.9^{+0.2}_{-0.2} \times 10^{-11}$ erg s^{-1} cm^{-2}	—
EP trigger ID 01709131775	80.748	−8.833	Associated with a T Tauri star RX J0523.0-0850, $F_{\rm peak} \approx 8.0 \times 10^{-11}$ erg s^{-1} cm^{-2}, corresponding to $L_X \approx 2.2 \times 10^{32}$ erg s^{-1}	—
EP trigger ID 01709131882	170.244	−38.768	Associated with a BY Dra Variable V1217 Cen, $F_{\rm peak} \approx 1.0 \times 10^{-10}$ erg s^{-1} cm^{-2}, corresponding to $L_X \approx 5.1 \times 10^{31}$ erg s^{-1}	—
			Fast X-ray Transients	
EP240305a	122.903	−54.657	Light curve shows double-peak profile. First flare: rise to $F_{\rm peak} \sim 5 \times 10^{-9}$ erg s^{-1} cm^{-2} (0.5–4.0 keV) in ∼100 s, decay to background ($\sim 1 \times 10^{-11}$ erg s^{-1} cm^{-2}) in ∼50 s. Second flare: rise to $F_{\rm peak} \sim 2.5 \times 10^{-9}$ erg s^{-1} cm^{-2} in ∼50 s, decay to background in ∼200 s. Averaged spectrum: absorbed power-law with $\Gamma = 1.6^{+0.5}_{-0.5}$, $N_H = 3.4^{+1.8}_{-1.7} \times 10^{21}$ cm^{-2}. $F_{\rm unabs} = 8.3^{+2.0}_{-1.4} \times 10^{-10}$ erg s^{-1} cm^{-2}	Maybe a late A or early F spectral-type star; radio counterpart detected
EP240331a	169.414	−20.042	Light curve: symmetric profile, Dur. ∼ 100 s. Spectrum: absorbed power-law with $\Gamma = 0.74^{+0.31}_{-0.30}$, $N_H = 3.44 \times 10^{20}$ cm^{-2} (fixed). $F_{\rm unabs} = 1.8^{+0.3}_{-0.3} \times 10^{-9}$ erg s^{-1} cm^{-2} (0.5–4 keV)	—
EP240408a	158.840	−35.749	Dur. ∼ 10 s. $F_{\rm peak} \sim 1.4 \times 10^{-8}$ erg s^{-1} cm^{-2} (0.5–4.0 keV). Spectrum: absorbed power-law with $\Gamma = 1.1^{+0.8}_{-0.7}$, $N_H = 6.23 \times 10^{20}$ cm^{-2} (fixed). $F_{\rm unabs} = 4.0^{+1.3}_{-1.3} \times 10^{-9}$ erg s^{-1} cm^{-2}.	Optical/NIR counterpart detected
EP240413a	228.794	−18.800	Dur. = 200 s, $F_{\rm peak} = 7 \times 10^{-9}$ erg s^{-1} cm^{-2}, $\Gamma = 1.6^{+0.1}_{-0.2}$, $N_H = 1.12 \times 10^{21}$ cm^{-2}, $F_{\rm unabs} = 1.1^{+0.1}_{-0.1} \times 10^{-9}$ erg s^{-1} cm^{-2}	If possible detection of the X-ray emission is true, EP240413a has faded by about 3 orders of magnitude in X-ray flux in about 14 h
EP240416a	203.150	−13.612	Dur. ≥ 200 s, $F_{\rm peak} = 1.3 \times 10^{-9}$ erg s^{-1} cm^{-2}, $N_H = 4.0 \times 10^{20}$ cm^{-2}, $\Gamma = 1.5^{+0.6}_{-0.6}$, $F_{\rm unabs} = 5.0^{+2.6}_{-1.6} \times 10^{-10}$ erg s^{-1} cm^{-2}	Optical counterpart candidate detected
EP240417a	177.442	−15.438	Dur. ≥ 1500 s, $F_{\rm peak} = 3 \times 10^{-10}$ erg s^{-1} cm^{-2}, $\Gamma = 1.15^{+0.27}_{-0.26}$, $N_H = 0$, $F_{\rm unabs} = 9.8^{+0.8}_{-0.8} \times 10^{-11}$ erg s^{-1} cm^{-2}	No other band counterparts
EP240420a	228.713	14.796	Dur. > 100 s, $F_{\rm peak} = 1 \times 10^{-8}$ erg s^{-1} cm^{-2}	Short-time X-ray flare; X-ray flux decays by 3 orders of magnitude in 2 h; optical counterpart detected
EP240426b	173.787	−40.741	Dur. = 300 s, $F_{\rm peak} = 9.5 \times 10^{-10}$ erg s^{-1} cm^{-2}, $\Gamma = 1.8^{+0.3}_{-0.3}$, $N_H = 8.08 \times 10^{20}$ cm^{-2}, $F_{\rm unabs} = 3.6^{+0.6}_{-0.6} \times 10^{-10}$ erg s^{-1} cm^{-2}	No multi-band counterpart; 40-degree deviation from S240422ed
EP240506a	213.978	−16.715	Dur. = 50 s, $F_{\rm peak} = 1 \times 10^{-8}$ erg s^{-1} cm^{-2}, $\Gamma = 1.0^{+0.5}_{-0.5}$, $N_H = 9.0 \times 10^{20}$ cm^{-2}, $F_{\rm unabs} = 1.1^{+0.3}_{-0.2} \times 10^{-9}$ erg s^{-1} cm^{-2}	No optical counterpart detected; possible background radio source
EP240518a	216.955	−49.565	Dur. > 1000 s, average $F = 8 \times 10^{-11}$ erg s^{-1} cm^{-2} (0.5–4 keV)	Possible stellar activity

Table 3. *Cont.*

Name	RA (deg)	Dec (deg)	X-Ray Properties	Notes
EP240618a	281.648	23.833	Dur. ≈ 100 s, $F_{\rm unabs,peak} = 1.5 \times 10^{-8}$ erg s^{-1} cm^{-2}, $\Gamma = 1.2^{+0.4}_{-0.4}$, $N_H = 1.98 \times 10^{21}$ cm^{-2}, $F_{\rm unabs,average} = 2.9^{+0.7}_{-0.6} \times 10^{-9}$ erg s^{-1} cm^{-2}	Optical candidate detected
EP240625a	310.760	−15.966	Dur. ≈ 300 s, $F_{\rm unabs,peak} = 1.3 \times 10^{-9}$ erg s^{-1} cm^{-2}, $\Gamma = 1.8^{+0.3}_{-0.3}$, $N_H = 3.85 \times 10^{20}$ cm^{-2}, $F_{\rm unabs,average} = 2.9^{+0.7}_{-0.5} \times 10^{-10}$ erg s^{-1} cm^{-2}	X-ray source decays slowly; optical candidate with low SNR detected
EP240626a	263.023	−13.051	Dur. ≈ 160 s, $F_{\rm unabs,peak} = 6 \times 10^{-9}$ erg s^{-1} cm^{-2}, $\Gamma = 0.95^{+0.54}_{-0.54}$, $N_H = 1.8 \times 10^{21}$ cm^{-2}, $F_{\rm unabs,average} = 1.70^{+0.73}_{-0.50} \times 10^{-9}$ erg s^{-1} cm^{-2}	Weak follow-up X-ray source detected; no optical counterpart
EP240702a	328.203	−38.980	Dur. ≈ 50 s, $F_{\rm peak} = 1.2 \times 10^{-8}$ erg s^{-1} cm^{-2}, $\Gamma = 1.1^{+0.2}_{-0.2}$, $N_H = 2.0 \times 10^{20}$ cm^{-2} (fixed), $F_{\rm unabs,average} = 5.4^{+1.5}_{-1.2} \times 10^{-9}$ erg s^{-1} cm^{-2}	No optical or radio counterpart; no matching known X-ray source
EP240703a	273.803	−9.681	Dur. ≈ 300 s, $F_{\rm peak} = 5 \times 10^{-9}$ erg s^{-1} cm^{-2} (absorbed), $N_H = 1.5^{+0.7}_{-0.6} \times 10^{22}$ cm^{-2}, $\Gamma = 2.0^{+1.0}_{-0.9}$, $F_{\rm unabs,average} = 5.9^{+8.6}_{-2.6} \times 10^{-9}$ erg s^{-1} cm^{-2}; When $N_H = 4.5 \times 10^{21}$ cm^{-2}, $\Gamma = 0.4^{+0.3}_{-0.3}$, $F_{\rm unabs,average} = 2.5^{+0.4}_{-0.3} \times 10^{-9}$ erg s^{-1} cm^{-2}	Optical candidate detected but not independently confirmed; no matching known X-ray source
EP240703b	279.539	−57.401	Dur. ≈ 600 s, $F_{\rm peak} = 3 \times 10^{-9}$ erg s^{-1} cm^{-2} (absorbed), $N_H = 1.4^{+1.3}_{-1.2} \times 10^{21}$ cm^{-2}, $\Gamma = 1.5^{+0.6}_{-0.5}$, $F_{\rm unabs,average} = 7.5^{+1.3}_{-1.8} \times 10^{-10}$ erg s^{-1} cm^{-2}; When $N_H = 6.8 \times 10^{20}$ cm^{-2}, $\Gamma = 1.2^{+0.2}_{-0.2}$, $F_{\rm unabs,average} = 7.1^{+1.1}_{-1.0} \times 10^{-10}$ erg s^{-1} cm^{-2}	No multi-band counterpart
EP240703c	289.264	−30.325	Dur. > 1000 s, with multipeak lightcurve structure, $N_H = 8 \times 10^{20}$ cm^{-2}, $\Gamma = 1.3^{+0.5}_{-0.5}$, $F_{\rm unabs} = 2.5^{+0.8}_{-0.8} \times 10^{-10}$ erg s^{-1} cm^{-2}	No clear multi-band counterpart; no matching known X-ray source
EP240708a	345.963	−22.840	Dur. ≈ 1300 s, $F_{\rm peak} = 1.1 \times 10^{-9}$ erg s^{-1} cm^{-2}, $N_H = 2.0 \times 10^{20}$ cm^{-2}, $\Gamma = 1.57^{+0.63}_{-0.54}$, $F_{\rm unabs,average} = 7.7^{+3.4}_{-2.6} \times 10^{-11}$ erg s^{-1} cm^{-2}	Weak follow-up X-ray source detected
EP240801a	345.140	32.610	Dur. > 80 s, lightcurve from WXT shows rapid brightening profile, $N_H = 3.1^{+3.1}_{-3.1} \times 10^{21}$ cm^{-2}, $\Gamma = 1.9^{+0.9}_{-0.9}$, $F_{\rm unabs,average} = 4.8^{+3.1}_{-3.1} \times 10^{-10}$ erg s^{-1} cm^{-2} (0.5–4 keV)	X-ray afterglow detected; optical candidate detected in the error circle, z = 1.673
EP240806a	11.491	5.091	Dur. ≈ 150 s, $N_H = 3.1^{-2.5}_{+2.8} \times 10^{21}$ cm^{-2}, $\Gamma = 2.6^{-1.0}_{+1.2}$, $F_{\rm unabs,average} = 1.9^{-0.6}_{+1.8} \times 10^{-9}$ erg s^{-1} cm^{-2}	Optical counterpart detected, z = 2.818
EP240816b	16.013	15.398	For the WXT: Dur. > 50 s, $N_H = 5.2 \times 10^{20}$ cm^{-2}, $\Gamma = 1.6^{+0.7}_{-0.7}$, $F_{\rm unabs,average} = 1.3^{+0.7}_{-0.5} \times 10^{-9}$ erg s^{-1} cm^{-2} (0.5–4 keV) For the average FXT spectrum in 0.5–10 keV band: $N_H = 9.5^{+6.9}_{-6.7} \times 10^{20}$ cm^{-2}, $\Gamma = 1.69^{+0.23}_{-0.22}$, $F_{\rm unabs,average} = 4.3^{+0.6}_{-0.5} \times 10^{-12}$ erg s^{-1} cm^{-2} (0.5–10 keV)	No clear optical or radio counterpart
EP240816a	292.925	−54.412	$N_H = 4.2 \times 10^{20}$ cm^{-2}, $\Gamma = 1.1^{+0.6}_{-0.5}$, $F_{\rm unabs,average} = 3.0^{+0.5}_{-0.5} \times 10^{-10}$ erg s^{-1} cm^{-2} For the average FXT spectrum in the 0.5–10 keV band: $N_H = 4.2 \times 10^{20}$ cm^{-2}, $\Gamma = 1.87^{+0.40}_{-0.39}$, $F_{\rm unabs,average} = 1.2^{+0.5}_{-0.3} \times 10^{-13}$ erg s^{-1} cm^{-2} (0.5–10 keV)	No multi-band counterpart
EP240820a	16.221	−34.698	For the WXT observed transient: Dur. ≈ 250 s, $N_H = 1.62 \times 10^{20}$ cm^{-2}, $\Gamma = 1.2^{-0.7}_{+0.8}$, $F_{\rm unabs,average} = 1.2^{-0.5}_{+0.7} \times 10^{-10}$ erg s^{-1} cm^{-2} (0.5–4 keV) For the FXT spectrum: Fitted with an absorbed power-law, parameters fixed to those from EP-WXT spectral fitting, $F \approx 2.0 \times 10^{-13}$ erg s^{-1} cm^{-2}	No multi-band counterpart

Table 3. *Cont.*

Name	RA (deg)	Dec (deg)	X-Ray Properties	Notes
EP240904a	276.8750	−9.9426	Detected by EP/WXT at 2024-09-04T17:20:40 UTC. WXT spectrum (0.5–4 keV): absorbed power-law with $\Gamma = 0.6^{+1.1}_{-1.3}$, $N_H = 1.32 \times 10^{22}$ cm^{-2} (fixed). $F_{\rm unabs} = 4.2^{+1.8}_{-1.6} \times 10^{-11}$ erg s^{-1} cm^{-2}. EP/FXT follow-up (5.9 ks exposure) localized source at R.A. = 276.8750°, Dec. = −9.9426° (J2000; 10 arcsec error radius). Spectrum (0.5–10 keV): $\Gamma = 1.95^{+0.01}_{-0.01}$, $N_H = 3.0^{+0.1}_{-0.1} \times 10^{22}$ cm^{-2}. $F_{\rm unabs} = 2.1^{+0.1}_{-0.1} \times 10^{-10}$ erg s^{-1} cm^{-2}.	Radio counterpart detected
EP240908a	14.0031	8.0735	For the WXT observed transient: Dur. ≈ 950 s, $F_{\rm peak} = 1 \times 10^{-9}$ erg s^{-1} cm^{-2} (0.5–4 keV), $N_H = 7 \times 10^{20}$ cm^{-2}, $\Gamma = 1.6^{-0.5}_{+0.4}$, $F_{\rm unabs,average} = 7.4^{-1.9}_{+2.4} \times 10^{-10}$ erg s^{-1} cm^{-2} (0.5–4 keV) For the FXT: $N_H = 1.5^{-1.5}_{+1.7} \times 10^{21}$ cm^{-2}, $\Gamma = 2.1^{-0.6}_{+0.7}$, $F_{\rm unabs}$(0.5–10.0 keV) = $7.4^{-2.0}_{+1.3} \times 10^{-13}$ erg s^{-1} cm^{-2}	Optical counterpart detected
EP240918a	289.3937	46.1281	For the WXT observed transient: Dur. ≈ 170 s, $F_{\rm peak} \approx 3.2 \times 10^{-9}$ erg s^{-1} cm^{-2}, $N_H = 9.9 \times 10^{20}$ cm^{-2}, $\Gamma = 1.7^{-0.6}_{+0.7}$, $F_{\rm unabs,average} = 7.2^{-1.9}_{+2.8} \times 10^{-10}$ erg s^{-1} cm^{-2} For the EP-FXT light curve: Shows a fast decline, flux decreased to ≈ 1.0×10^{-13} erg s^{-1} cm^{-2} within ≈ 1000 s	No clear optical or radio counterpart
EP240918b	258.66	66.739	Dur. ≈ 200 s, $F_{\rm absorbed,average}$ = $2.6^{+4.1}_{-1.2} \times 10^{-10}$ erg s^{-1} cm^{-2}, $N_H = 3.2^{+6.2}_{-3.2} \times 10^{21}$ cm^{-2}, $\Gamma = 1.5^{+1.8}_{-1.3}$	No clear optical or radio counterpart
EP240918c	281.338	−13.167	Dur. ≈ 100 s, $F_{\rm peak} \approx 5.8 \times 10^{-9}$ erg s^{-1} cm^{-2} (0.5–4 keV), $N_H = 3.7 \times 10^{21}$ cm^{-2}, $\Gamma = 1.6^{+0.8}_{-0.8}$, $F_{\rm unabs,average} = 1.5^{+0.6}_{-0.2} \times 10^{-9}$ erg s^{-1} cm^{-2}	No previously known bright X-ray sources are found within the error circle around the source position
EP241021a	28.852	5.957	$F_{\rm peak} \approx 1 \times 10^{-9}$ erg s^{-1} cm^{-2} (0.5–4 keV), $N_H = 5 \times 10^{20}$ cm^{-2}, $\Gamma = 1.48^{-1.22}_{+1.24}$, $F_{\rm unabs,average} = 3.3^{-1.6}_{+4.8} \times 10^{-10}$ erg s^{-1} cm^{-2}	Optical counterpart detected; redshift of host galaxy $z = 0.748$; a bright source was detected at the optical transient (OT) position at a frequency of 5.5 GHz; the flux density of this source is 400^{+20}_{-20} μJy
EP241026b	56.403	41.031	$F_{\rm peak} \approx 1.7 \times 10^{-9}$ erg s^{-1} cm^{-2} (0.5–4 keV), $N_H = 3.38 \times 10^{21}$ cm^{-2}, $\Gamma = 2.5^{+0.8}_{-0.8}$, $F_{\rm unabs,average} = 1.2^{-0.3}_{+0.4} \times 10^{-10}$ erg s^{-1} cm^{-2}	Short-time X-ray flare; optical candidate with 1.9-magnitude brightening detected; an upper limit of 1.8 for the redshift
EP241101a	37.763	22.731	For the WXT observed transient: Dur. > 100 s, $N_H = 1.5 \times 10^{21}$ cm^{-2}, $\Gamma = 0.9^{+0.6}_{-0.6}$, $F_{\rm unabs,average} = 1.2^{+0.5}_{-0.4} \times 10^{-9}$ erg s^{-1} cm^{-2} (0.5–4 keV) For the FXT: During its autonomous observation within the WXT error circle, no significant source was detected. The flux upper limit is 7.1×10^{-14} erg s^{-1} cm^{-2} (0.5–10 keV)	Possible detection of some optical counterparts
EP241103a	27.7572	18.9587	For the WXT: Duration: ≈ 60 s, $N_H = 6.3 \times 10^{20}$ cm^{-2}, $\Gamma = 0.8^{+0.4}_{-0.4}$, $F_{\rm unabs,average} = 3.8^{+1.1}_{-0.9} \times 10^{-9}$ erg s^{-1} cm^{-2}, $F_{\rm peak} \approx 1.1 \times 10^{-8}$ erg s^{-1} cm^{-2} For FXT (in the 0.5–10 keV band): Exposure time: 2300 s, no significant light curve variation observed, N_H fixed at Galactic value, $\Gamma = 2.0^{+0.4}_{-0.4}$, $F_{\rm average} = 6.0^{+2.3}_{-1.4} \times 10^{-13}$ erg s^{-1} cm^{-2}	No multi-band counterpart
EP241107a	35.0085	3.3329	The trigger flux: ≈ 1×10^{-10} erg s^{-1} cm^{-2}	Optical and radio (the flux density is 207^{+7}_{-7} μJy) counterpart candidates detected; z = 0.456
EP241113a	131.9964	52.3815	WXT Observations: - $\Gamma = 1.3 \pm 0.2$, $N_H = 2.6 \times 10^{20}$ cm^{-2} - $F_{\rm avg}$: $5.57^{+1.26}_{-0.76} \times 10^{-10}$ erg s^{-1} cm^{-2} FXT Observations: Exp. time: 5000 s, significant decline in light-curve, $\Gamma = 2.40 \pm 0.17$, N_H fixed - $F_{\rm avg}$ in 0.5–10 keV: $2.5^{+0.3}_{-0.2} \times 10^{-11}$ erg s^{-1} cm^{-2}	X-ray fading, no gamma-ray counterpart; tentative host redshift $z = 1.53$, likely extragalactic origin

Table 3. *Cont.*

Name	RA (deg)	Dec (deg)	X-Ray Properties	Notes
EP241119a	84.116	3.832	By WXT: Dur. $\approx 200\,s$, $F_{\rm peak} \approx 4 \times 10^{-9}$ erg s^{-1} cm^{-2}. $\Gamma = 1.27^{+0.45}_{-0.44}$, $N_H = 2.1 \times 10^{21}$ cm^{-2}, $F_{\rm unabs} = 2.43^{+0.67}_{-0.52} \times 10^{-10}$ erg s^{-1} cm^{-2} (0.5–4 keV). 9 h later by FXT, $F_{\rm AG} \approx 2 \times 10^{-13}$ erg s^{-1} cm^{-2}.	No multi-band association or optical candidate detected
EP241125a	48.561	37.677	Dur. > 150 s, $F_{\rm peak} \approx 8 \times 10^{-10}$ erg s^{-1} cm^{-2} (0.5–4 keV). $\Gamma = 1.90^{+1.12}_{-0.95}$, $N_H = 1.2 \times 10^{21}$ cm^{-2} (fixed), $F_{\rm unabs} = 2.79^{+1.11}_{-0.86} \times 10^{-10}$ erg s^{-1} cm^{-2}.	No multi-band association
EP241126a	33.744	11.705	Dur. > 60 s, $F_{\rm peak} \approx 2 \times 10^{-8}$ erg s^{-1} cm^{-2} (0.5–4 keV). $\Gamma = 0.9^{+0.4}_{-0.4}$, $N_H = 7.4 \times 10^{20}$ cm^{-2} (fixed), $F_{\rm unabs} = 3.3^{+0.9}_{-0.7} \times 10^{-9}$ erg s^{-1} cm^{-2} (0.5–4 keV).	Optical counterpart detected
EP241201a	282.596	66.081	Dur. ≈ 230 s, $\Gamma = 3.9^{-1.4}_{+1.6}$, $N_H = 1.5^{-0.6}_{+0.8} \times 10^{22}$ cm^{-2}, $F_{\rm unabs} = 7.1^{-4.9}_{+32.7} \times 10^{-9}$ erg s^{-1} cm^{-2}	Optical candidate detected
EP241202b	45.302	2.441	Dur. > 140 s, $F_{\rm peak} = 1.4 \times 10^{-9}$ erg s^{-1} cm^{-2}. $\Gamma = 1.06^{+0.43}_{-0.41}$, $N_H = 9.5 \times 10^{20}$ cm^{-2}, $F_{\rm unabs} = 5.4^{+2.0}_{-1.6} \times 10^{-10}$ erg s^{-1} cm^{-2}	Optical candidate detected
EP241206a	34.702	38.914	Dur. ≈ 400 s. $\Gamma = 1.96^{+0.52}_{-0.40}$, $N_H = 5.47 \times 10^{20}$ cm^{-2} (fixed), $F_{\rm unabs} = 4.92^{+1.19}_{-1.24} \times 10^{-10}$ erg s^{-1} cm^{-2}	No multi-band counterpart detected
EP241208a	127.812	49.082	Dur. ≈ 50 s (trigger ID: 01709128715). $\Gamma = 1.29^{+0.93}_{-0.88}$, $N_H = 4.20 \times 10^{20}$ cm^{-2} (fixed), $F_{\rm unabs} = 6.57^{+4.73}_{-2.49} \times 10^{-10}$ erg s^{-1} cm^{-2}	The long soft transient also was detected by SVOM
EP241217a	46.957	30.901	$F_{\rm peak\,count} \approx 1$ cnt/s. In 0.5–4 keV, $\Gamma = 1.93^{+0.71}_{-0.59}$ (absorbed power-law), $F_{\rm unabs} = (7.3 \pm 2.7) \times 10^{-10}$ erg s^{-1} cm^{-2}. FXT follow-up: at 1.02 h post-trigger, $F_{0.5-10{\rm keV}} = (6.23 \pm 0.46) \times 10^{-12}$ erg s^{-1} cm^{-2}; at 8.18 h post-trigger, $F_{0.5-10{\rm keV}} = (1.35 \pm 0.22) \times 10^{-12}$ erg s^{-1} cm^{-2}. Flux decay index $\alpha = 0.73 \pm 0.35$, consistent with Swift-XRT. Spectral fits: negligible intrinsic absorption, $\Gamma_1 = 1.76 \pm 0.11$, $\Gamma_2 = 1.96 \pm 0.17$.	Optical candidate detected; z = 4.59; radio counterpart (the flux densities are 20 ± 6.6 μJy at 3 GHz, 58 ± 4 μJy at 6 GHz, and 99.3 ± 4.1 μJy at 10 GHz)
EP241223a	74.804	7.110	Dur. ≈ 80 s, $F_{\rm peak} \approx 2.4 \times 10^{-9}$ erg s^{-1} cm^{-2}, $\Gamma = 2.01^{+1.02}_{-0.85}$, $N_H = 1.22 \times 10^{21}$ cm^{-2} (fixed), $F_{\rm unabs} = 9.0^{+4.0}_{-4.0} \times 10^{-10}$ erg s^{-1} cm^{-2}	No optical counterpart or other multi-band association detected
EP241231b	100.064	16.171	$F_{\rm abs}$ (absorbed flux) $= 1.5^{+1.1}_{-0.5} \times 10^{-10}$ erg s^{-1} cm^{-2}, $N_H = 4.1 \times 10^{21}$ cm^{-2} (fixed), $\Gamma = 2.1^{+1.1}_{-0.9}$	No multi-band association or optical candidate detected
EP250101a	85.575	0.352	Dur. $\approx 2500\,s$ is seen. $F_{\rm peak} \approx 1.7 \times 10^{-10}$ erg s^{-1} cm^{-2}, $\Gamma = 1.5^{+1.6}_{-1.1}$, $N_H = 3.3 \times 10^{21}$ cm^{-2} (fixed), $F_{\rm unabs} = 4.4^{+2.3}_{-1.7} \times 10^{-11}$ erg s^{-1} cm^{-2}	No optical counterpart or other multi-band association detected
EP250109b	118.611	−14.651	Peak flux (0.5–4 keV) = $\sim 7 \times 10^{-10}$ erg s^{-1} cm^{-2}, photon index (average 0.5–4 keV spectrum during flare) = $1.5^{+1.2}_{-1.1}$ (galactic column density fixed at 1.68×10^{21} cm^{-2}), average unabsorbed 0.5–4 keV flux = $(3.0^{+2.3}_{-1.2}) \times 10^{-10}$ erg s^{-1} cm^{-2}	Distance error circle of the nearby eclipsing binary MT Pup is 3.6 arcminutes (exceeding the positioning uncertainty range), and the flare luminosity ($>10^{34}$ erg/s) is much higher than that of a typical stellar flare (usually $<10^{32}$ erg/s)
EP250111a	97.1809	56.8983	Dur. $= 83$ s, $N_H = 1.11 \times 10^{21}$ cm^{-2} (fixed), $\Gamma = 1.01^{-0.52}_{+0.54}$, $F_{\rm obs} = 1.39^{-0.40}_{+0.53} \times 10^{-9}$ erg s^{-1} cm^{-2} About 4 min later, FXT autonomous observation. For FXT 0.5–10 keV: Fitted with absorbed power-law, $N_H = 1.11 \times 10^{21}$ cm^{-2} (fixed), $\Gamma = 2.42^{-0.14}_{+0.15}$, $F_{\rm obs} = 3.43^{-0.33}_{+0.36} \times 10^{-12}$ erg s^{-1} cm^{-2} (0.5–10 keV).	Optical candidate detected

Table 3. *Cont.*

Name	RA (deg)	Dec (deg)	X-Ray Properties	Notes
EP250125a	175.364	−21.708	For WXT, Dur. = 74 s, $N_H = 4.15 \times 10^{20}$ cm^{-2} (fixed), $\Gamma = 0.8^{-0.5}_{+0.5}$, $F_{\rm unabs} = 1.8^{-0.5}_{+0.7} \times 10^{-9}$ erg s^{-1} cm^{-2} (0.5–4 keV). About 2 min later, FXT autonomous observation. For FXT 0.5–10 keV: Fitted with absorbed power-law, $N_H = 4.15 \times 10^{20}$ cm^{-2} (fixed), $\Gamma = 2.0^{-0.1}_{+0.1}$, $F_{\rm unabs} = 5.4^{-0.6}_{+0.6} \times 10^{-12}$ erg s^{-1} cm^{-2} (0.5–10 keV).	Presence of optical candidates (at r = 19.3 mag); z = 2.89
EP250207b	167.495	−7.906	Dur. > 120 s (before observation ended). For WXT, $N_H = 4.24 \times 10^{20}$ cm^{-2} (fixed), $\Gamma = 0.6^{-0.8}_{+0.8}$, $F_{\rm unabs} = 6.1^{-2.5}_{+4.2} \times 10^{-10}$ erg s^{-1} cm^{-2}. FXT conducted two ToO observations: First observation: For FXT 0.5–10 keV, $N_H = 4.24 \times 10^{20}$ cm^{-2}, $\Gamma = 1.5^{-0.6}_{+0.6}$, $F_{\rm unabs} = 3.6^{-1.4}_{+3.5} \times 10^{-13}$ erg s^{-1} cm^{-2} (0.5–10 keV). Second observation: $F = 6.4^{-2.8}_{+3.5} \times 10^{-14}$ erg s^{-1} cm^{-2} (flux declined)	Optical candidate detected; needs follow-up; not verified by other observations
EP250212a	114.949	60.493	Dur. ≈ 360 s (from WXT light curve), $N_H = 0.5^{-0.3}_{+0.3} \times 10^{22}$ cm^{-2}, $\Gamma = 2.2^{-0.9}_{+1.0}$, $F_{\rm unabs} = 0.9^{-0.3}_{+1.0} \times 10^{-9}$ erg s^{-1} cm^{-2}, $F_{\rm peak} \approx 6 \times 10^{-9}$ erg s^{-1} cm^{-2}. (absorbed blackbody): $N_H^{\rm upper\ limit} = 0.45 \times 10^{22}$ cm^{-2}, $T = 0.6^{-0.1}_{+0.2}$ keV. EP-FXT follow-up ToO observation: Exposure time $t = 5970$ s, about 5.6 h after EP-WXT detection. For FXT 0.5–10 keV (absorbed power-law): $N_H = 6.3 \times 10^{20}$ cm^{-2} (fixed), $\Gamma = 2.1^{-0.3}_{+0.3}$, $F_{\rm unabs} = 3.2^{-0.7}_{+0.8} \times 10^{-13}$ erg s^{-1} cm^{-2}.	No optical counterpart or other multi-band association detected
EP250220a	113.400	39.795	Dur. ≈ 150 s, $N_H = 7.13 \times 10^{20}$ cm^{-2} (fixed), $\Gamma = 1.8^{-0.9}_{+1.0}$, $F_{\rm unabs} = 5.8^{-2.2}_{+3.3} \times 10^{-11}$ erg s^{-1} cm^{-2}. First FXT observation: 13 h after WXT detection, exposure ∼ 3 ks. In the WXT error circle, an FXT module detected a faint X-ray source. Second FXT observation: 32 h after WXT detection, exposure ∼ 7 ks. No source in the WXT error circle. With $\Gamma = 1.1$, $N_H = 7.13 \times 10^{20}$ cm^{-2}, 0.5–10 keV upper limit is 1.90×10^{-14} erg s^{-1} cm^{-2}.	No optical counterpart or other multi-band association detected
EXO 0748-676/UY Vol	117.140458	−67.752138	EXO 0748-676/UY Vol exhibited renewed X-ray activity with multiple Type-I bursts detected since June 2024, ending its 16-year quiescence since 2008. EP-WXT initially detected the source on 9 July 2024 (26 ks exposure) with $F_{\rm unabs} \sim 2.2 \times 10^{-12}$ erg s^{-1} cm^{-2} (0.5–4 keV; $\Gamma = -2.0$ fixed, $N_H = 1.5 \times 10^{21}$ cm^{-2}). Subsequent non-detections in July–August 2024 set $F_{\rm upper} < 7.7 \times 10^{-12}$ erg s^{-1} cm^{-2}. Renewed brightening was observed from 2024-10-04T22:42:34 UTC onward, with $F_{\rm unabs}$ increasing from 2.4×10^{-11} to 4.5×10^{-11} erg s^{-1} cm^{-2} (0.5–4 keV), indicating ∼20× flux enhancement compared to July levels.	Neutron star thermonuclear bursts
Optical Transients				
EP240414a	191.498	−9.695	WXT: $F_{\rm peak} = 3 \times 10^{-9}$ erg s^{-1} cm^{-2} FXT: $N_H = 3.35 \times 10^{20}$ cm^{-2} (fixed), $\Gamma = 1.7^{+0.3}_{-0.3}$, $F_{\rm unabs} = 3.5^{+0.8}_{-0.8} \times 10^{-13}$ erg s^{-1} cm^{-2} (0.5–10 keV), associated with EP240414a, faded by 4 orders of magnitude in X-ray flux in 2 h since WXT detection	Optical counterpart AT2024gsa detected; later spectral evolution to SN Ic-BL; radio detection similar to long GRB

Table 3. *Cont.*

Name	RA (deg)	Dec (deg)	X-Ray Properties	Notes
EP240426a	121.8567	−29.4609	Assuming a power-law spectrum with $\Gamma = 2.0$ and galactic absorption, $F_{\rm unabs} = 9.2 \times 10^{-13}$ erg s^{-1} cm^{-2} (0.5–10 keV)	As an optical counterpart reported by DECam, AT 2024hfq shows obvious optical excitation characteristics, which is consistent with the electromagnetic counterpart in the context of multiple messengers. At the same time, the X-ray signal detected by EP-FXT is auxiliary information, which supports that the event is related to the merger of compact objects triggered by gravitational waves
EP250108a	55.623	−22.509	Dur. > 2500 s. $F_{\rm peak} \sim 1.4 \times 10^{-10}$ erg s^{-1} cm^{-2} (0.5–4 keV). Spectrum: absorbed power-law with $\Gamma = 1.35 \pm 0.40$, $N_H = 1.6 \times 10^{20}$ cm^{-2} (fixed). $F_{\rm unabs} = 4.2^{+1.2}_{-0.9} \times 10^{-11}$ erg s^{-1} cm^{-2}	Associated with optical counterpart AT 2025kg, redshift $z = 0.176$
EP250223a	98.258	−22.432	WXT: Dur. = 140 s, $F_{\rm peak} = 2 \times 10^{-9}$ erg s^{-1} cm^{-2}, $N_H = 1.36 \times 10^{21}$ cm^{-2} (fixed), $\Gamma = 2.1^{\pm 0.6}$, $F_{\rm unabs} = 4.4^{-1.1}_{+1.4} \times 10^{-10}$ erg s^{-1} cm^{-2}. FXT: About 2 min later, for FXT 0.5–10 keV, $N_H = 1.36 \times 10^{21}$ cm^{-2}, $\Gamma = 1.97^{\pm 0.05}$, $F_{\rm unabs} = 2.5^{\pm 0.1} \times 10^{-11}$ erg s^{-1} cm^{-2}.	Optical counterpart detected, z = 2.756
Known Sources/Unclassified				
EP240309a	178.566	−50.29	WXT detected persistent emission (16 March 2024 before) with $F_{\rm peak} = 5$–7×10^{-12} erg s^{-1} cm^{-2} (0.5–4 keV), upper limit 9.4×10^{-12} erg s^{-1} cm^{-2} (17 March 2024). Historical detections: XMMSL J115415.6-501758 ($F_{\rm peak} = 3.5 \times 10^{-12}$ erg s^{-1} cm^{-2}, 0.2–2 keV; 10 January 2022), Swift/XRT (1.5×10^{-11} erg s^{-1} cm^{-2}, 0.3–10 keV; 20 July 2021), 1eRASS J115415.7-501758 (3.0×10^{-14} erg s^{-1} cm^{-2}, 0.2–2.3 keV FXT spectrum: $\Gamma = 0.95^{+0.31}_{-0.25}$, $N_H = 3.3^{+2.0}_{-1.3} \times 10^{21}$ cm^{-2}, $F_{\rm unabs} = 7.4 \times 10^{-12}$ erg s^{-1} cm^{-2} (0.3–10 keV). Spatial association with highly variable UV/optical source Gaia DR3 5370642890382757888 ($g = 14$–17; offset < 10 arcsec), suggesting Galactic CV's origin	Galactic CV candidate
EP240327a	203.853	7.488	Spectrum: absorbed blackbody (tbabs * bbody) with $N_H = 2.7 \times 10^{20}$ cm^{-2} (fixed), $kT = 79^{+18}_{-15}$ eV. $F_{\rm unabs} = 3.5^{+0.9}_{-0.9} \times 10^{-12}$ erg s^{-1} cm^{-2} (0.5–4.0 keV). Source associated with nucleus of early-type galaxy SDSS J133519.91 + 072,807.4 ($z = 0.0024$)	Possible AGN flare
GOTO065054.49 + 593,624.51	102.7272	59.6078	Spectrum (0.5–10 keV): absorbed power-law with $\Gamma = 3.23^{+0.68}_{-0.56}$, $N_H = 7.1^{+6.8}_{-4.3} \times 10^{20}$ cm^{-2}. $F_{\rm unabs} = 8.1^{+1.9}_{-1.4} \times 10^{-14}$ erg s^{-1} cm^{-2}	Galactic WZ Sge-type dwarf nova outburst (high-amplitude optical/X-ray transient; spectra confirm Balmer/HeI absorption lines)
EP J0052.9-7230	13.215	−72.494	Associated with CXOU J005245.0-722844, WXT spectra (0.5–4 keV): absorbed blackbody with $T = 0.087^{+0.002}_{-0.002}/0.091^{+0.001}_{-0.001}$ keV, $N_H = 4.8 \times 10^{21}$ cm^{-2} (fixed). Corresponding $F_{\rm unabs} = 1.76^{+0.08}_{-0.08}/1.52^{+0.05}_{-0.05} \times 10^{-9}$ erg s^{-1} cm^{-2}	Potential neutron star/white dwarf origin
EP240709a	7.910	−56.760	WXT spectrum (0.5–4 keV): absorbed power-law with $\Gamma = 0.7^{+0.6}_{-0.6}$, $N_H = 1.2 \times 10^{20}$ cm^{-2} (fixed). $F_{\rm unabs} = 1.3^{+0.6}_{-0.5} \times 10^{-11}$ erg s^{-1} cm^{-2}. FXT follow-up observation Spectrum: $\Gamma = 2.3^{+0.1}_{-0.2}$, $N_H = 1.5^{+0.4}_{-0.4} \times 10^{21}$ cm^{-2}. $F_{\rm unabs} = 6.6^{+0.3}_{-0.3} \times 10^{-12}$ erg s^{-1} cm^{-2} (0.5–10 keV).	Associated with high-energy gamma-ray source 4FGL J0031.5-564

Table 3. *Cont.*

Name	RA (deg)	Dec (deg)	X-Ray Properties	Notes
CV GD 1662	352.248	−29.749	Historical Swift/XRT observations show high variability: $F_{\rm unabs} = 1.3^{+0.3}_{-0.3} \times 10^{-13}$ erg s^{-1} cm^{-2} (17 October 2008) vs. $2.4^{+0.1}_{-0.1} \times 10^{-12}$ erg s^{-1} cm^{-2} (10 August 2015; 0.5–10 keV). FXT spectrum: absorbed power-law with $\Gamma = 1.63^{+0.09}_{-0.09}$. $F_{\rm unabs} = 4.65^{+0.21}_{-0.21} \times 10^{-12}$ erg s^{-1} cm^{-2}	CV flare activity
HMXB 4U 2238 + 60	339.8390	61.2729	EP/WXT detected $F_{\rm obs} \sim 1.0 \times 10^{-11}$ erg s^{-1} cm^{-2}. EP/FXT follow-up (2421 s exposure) localized source at R.A. = 339.8390°, Dec. = 61.2729° (10 arcsec error radius; Assoc.: HMXB 4U 2238 + 60, 5.5 arcsec from Gaia EDR3). Historical Chandra detection (2013): $F_{\rm unabs} = 3.8^{+0.4}_{-0.4} \times 10^{-13}$ erg s^{-1} cm^{-2} (0.5–7 keV). FXT spectrum: $\Gamma = 0.8^{+0.2}_{-0.2}$, $F_{\rm unabs} = 5.4^{+0.4}_{-0.4} \times 10^{-11}$ erg s^{-1} cm^{-2} (0.5–10 keV), indicating a ∼140× flux increase	HMXB outburst
PHL 1811	328.756302	−9.373429	EP/WXT detected a flare from quasar PHL 1811 (9.24 ks exposure), $F_{\rm unabs} = 1.2^{+0.7}_{-0.7} \times 10^{-11}$ erg s^{-1} cm^{-2} (0.5–4 keV). EP/FXT follow-up (2024-08-04T14:35:25 UTC, 33 h later) confirmed association, with $\Gamma = 1.85^{+0.29}_{-0.29}$ and $F_{\rm unabs} = 5.25^{+0.15}_{-0.15} \times 10^{-13}$ erg s^{-1} cm^{-2} (0.5–10 keV). Swift/XRT non-detection (2024-08-06T20:45:02 UTC) sets $F_{\rm upper} < 1.0 \times 10^{-13}$ erg s^{-1} cm^{-2} (0.3–10 keV). Historical fluxes: $6.8^{+0.4}_{-0.4} \times 10^{-14}$ erg s^{-1} cm^{-2} (XMM-Newton 1 November 2004; 0.2–12 keV), $4.2^{+1.0}_{-1.0} \times 10^{-13}$ erg s^{-1} cm^{-2} (Swift/XRT 22 October 2005; 0.3–10 keV). EP flare shows ∼100× flux enhancement, indicating day-timescale X-ray variability in this X-ray weak WLQ	Quasar X-ray flare
Aql X-1	287.816905	0.584963	Detected by EP-WXT: Power-law: $\Gamma = 2.7^{+1.6}_{-1.1}$, $N_H = 1.6^{+0.9}_{-0.7} \times 10^{22}$ cm^{-2}, $F_{\rm unabs} = 2.1^{+6.5}_{-1.1} \times 10^{-10}$ erg s^{-1} cm^{-2} (0.5–4 keV); Diskbb: $kT = 0.8^{+0.6}_{-0.3}$ keV, $N_H = 1.1^{+0.3}_{-0.4} \times 10^{22}$ cm^{-2}, $F_{\rm unabs} = 1.1^{+0.6}_{-0.3} \times 10^{-10}$ erg s^{-1} cm^{-2}. 2024-09-18T15:53:42 UTC (flux increased): Power-law: $\Gamma = 1.9^{+0.2}_{-0.3}$, $N_H = 1.0^{+0.1}_{-0.2} \times 10^{22}$ cm^{-2}, $F_{\rm unabs} = 6.0^{+1.1}_{-0.7} \times 10^{-10}$ erg s^{-1} cm^{-2}; Diskbb: $kT = 1.1^{+0.2}_{-0.1}$ keV, $N_H = 0.7^{+0.1}_{-0.1} \times 10^{22}$ cm^{-2}, $F_{\rm unabs} = 4.7^{+0.4}_{-0.4} \times 10^{-10}$ erg s^{-1} cm^{-2}	LMXB accretion state transition
S241125n	58.079	+69.689	Duration = Following the gravitational wave event S241125n and the Swift/BAT candidate, EP/FXT conducted an 11 ks observation of the BAT localization region (R.A. = 58.079°, Dec. = +69.689°) 26 h post-trigger. Within the 5 arcmin error circle, an X-ray source EPF_J035226 + 6938 (R.A. = 58.1097°, Dec. = 69.6392°, 10 arcsec positional uncertainty) was detected, consistent with the Swift/XRT source S241125n_X3 (GCN 38324). Its spectrum is well fitted by a power-law model with $\Gamma = 0.43^{+0.76}_{-0.74}$ ($N_H = 3.4 \times 10^{21}$ cm^{-2} fixed), yielding $F_{\rm unabs} = 1.17^{+1.18}_{-0.63} \times 10^{-13}$ erg s^{-1} cm^{-2} (0.5–10 keV). Six additional X-ray sources were detected within a 10 arcmin radius, including three cross-matched with Swift/XRT. The brightest source, EPF_J035113 + 6949, has an observed flux of $\sim 7.7 \times 10^{-13}$ erg s^{-1} cm^{-2}	Gravitational wave counterpart candidate

Table 3. *Cont.*

Name	RA (deg)	Dec (deg)	X-Ray Properties	Notes
RX J0032.9-7348	8.232	−37.807	Detected possible X-ray brightening of HMXB RX J0032.9-7348 (SMC) on 2024-10-27T19:36:51 UTC (5.6 ks exposure), localized at R.A. = 8.232°/−73.807° (2.2 arcmin error). Follow-up EP/FXT observations (14.5/20.9 h post-detection) confirmed a source at R.A. = 8.2249°/−73.8094° (10 arcsec precision; Assoc.: RX J0032.9-7348, 3.6 arcsec offset from Haberl & Sturm, 2016 position). Time-resolved FXT spectra show $\Gamma = 0.81^{+0.05}_{-0.05}$, $N_H = 4.8^{+2.5}_{-2.4} \times 10^{20}$ cm^{-2}, $F_{\rm unabs} = 7.95^{+0.31}_{-0.30} \times 10^{-11}$ erg s^{-1} cm^{-2} (0.5–10 keV), ∼40× brighter than historical upper limits (RASS 1993: $\sim 2 \times 10^{-12}$ erg s^{-1} cm^{-2}; XMM-Newton/Swift 2010–2024: $< 10^{-12}$ erg s^{-1} cm^{-2}), indicating a potential outburst	HMXB potential outburst
LAMOST J015016.17 + 375,618.9	27.556	37.937	Detected X-ray brightening of CV LAMOST J015016.17 + 375,618.9 on 2024-11-05T07:13:32 UTC (11.8 ks exposure), localized at R.A. = 27.556°/+37.937° (2.3 arcmin uncertainty). Stacked pre-flare data (7 September 2024) sets $F_{\rm upper} \sim 2 \times 10^{-12}$ erg s^{-1} cm^{-2}. WXT spectrum: $\Gamma = 1.3^{+0.7}_{-0.4}$ ($N_H = 5.2 \times 10^{20}$ cm^{-2} fixed), $F_{\rm unabs} = 7.2^{+2.7}_{-2.7} \times 10^{-12}$ erg s^{-1} cm^{-2} (0.5–4 keV). EP/FXT follow-up (2024-11-06T08:52:05 UTC) confirmed the source at R.A. = 27.5677°/+37.9381° (10 arcsec precision; Assoc.: CV LAMOST J015016.17 + 375,618.9, 1.9 arcsec offset) with $\Gamma = 1.53^{+0.10}_{-0.08}$, $F_{\rm unabs} = 7.83^{+0.21}_{-0.21} \times 10^{-12}$ erg s^{-1} cm^{-2} (0.5–10 keV), ∼40× brighter than ROSAT All-Sky Survey flux ($\sim 2 \times 10^{-13}$ erg s^{-1} cm^{-2})	CV outburst
QX Nor	243.162	−52.404	Detected possible X-ray brightening of LMXB QX Nor (1.6 ks exposure). Spectrum: absorbed power-law with $\Gamma = 1.3^{+0.5}_{-0.4}$, $N_H = 9.60^{+2.73}_{-2.35} \times 10^{21}$ cm^{-2}. $F_{\rm unabs} = 1.0^{+0.4}_{-0.2} \times 10^{-9}$ erg s^{-1} cm^{-2} (0.5–4 keV).	LMXB accretion flare
EP J064833.4 + 065,624	102.133	6.919	Detected a new X-ray outburst (EP J064833.4 + 065,624) associated with CV PNV J06483343 + 0,656,236 . WXT spectrum: $\Gamma = 4.5^{+2.7}_{-2.1}$ ($N_H = 5.5 \times 10^{21}$ cm^{-2} fixed), $F_{\rm abs} = 6.0^{+6.6}_{-3.2} \times 10^{-12}$ erg s^{-1} cm^{-2} (0.5–4 keV). Follow-up EP/FXT (2025-02-10T18:11:45 UTC) localized source at R.A. = 102.1393°/Dec. = 6.9401° (10 arcsec precision; Assoc.: PNV J06483343+0656236, 1.3 arcsec offset) with $\Gamma = 1.54^{+0.15}_{-0.11}$, $N_H < 6.5 \times 10^{20}$ cm^{-2}, $F_{\rm unabs} = 1.36^{+0.13}_{-0.12} \times 10^{-11}$ erg s^{-1} cm^{-2} (0.5–10 keV; ∼40× brighter than ROSAT $F_{\rm peak} \sim 3.5 \times 10^{-13}$). Coincident optical outburst observed since 29 January 2025 with $\Delta g \sim 4.8$ mag brightening (ASAS-SN). First X-ray detection from this CV.	CV outburst with optical counterpart

Note: In the fourth column, the following abbreviations and conventions are used: RA/Dec—Right Ascension and Declination (in degrees, J2000 epoch). EP—*Einstein Probe*. Dur.—Duration (seconds); values correspond to the first exposure relative to the X-ray trigger time. $F_{\rm peak}$—Peak flux in the 0.5–4 keV band (erg s^{-1} cm^{-2}). $F_{\rm AG}$—Afterglow flux in the 0.5–4 keV band (erg s^{-1} cm^{-2}), based on the first exposure. N_H—Hydrogen column density (cm^{-2}); "fixed" indicates that the value was held constant during spectral fitting. Γ—Photon index of the power-law spectrum. $F_{\rm unabs}$—Unabsorbed flux in the 0.5–4 keV band (erg s^{-1} cm^{-2}). T—Temperature (keV), as derived from the absorbed apec model. abs apec—Absorbed Astrophysical Plasma Emission Code model (thermal plasma emission); the model assumes fixed metal abundances and follows standard fitting procedures. Assoc.—"Associated with", indicating source classifications (e.g., M-type star, GRB, FXT, OT). X-ray L_jump—X-ray luminosity jump, representing the factor by which the X-ray luminosity increases relative to the

quiescent state. WXT—Wide-field X-ray Telescope of the *Einstein Probe*. FXT—Follow-up X-ray Telescope of the *Einstein Probe*. Fixed parameters—Values marked as "fixed" were not varied during spectral fitting, typically based on prior constraints (e.g., Galactic absorption). Energy range—Unless specified, fluxes are reported in the 0.5–4 keV band. Upper limit—3σ flux upper limit in the 0.5–4 keV band (erg s^{-1} cm^{-2}). Uncertainties represent 1 σ errors unless otherwise noted. For missing or inapplicable data, a dash (—) is used. The coordinates listed in this table and the corresponding X-ray properties are based primarily on the initial reports provided by *EP* for each source. When a source's coordinates are not available from the *EP* report, the coordinates from the SIMBAD catalog have been added. Furthermore, source names follow the official *EP* nomenclature whenever available; if no official *EP* name exists, the source is instead identified by the corresponding star's name.

Table A1 in the Appendix A provides a detailed summary of the multi-wavelength follow-up observations for transient events whose names begin with "*EP*". These sources are selected because they represent the initial detections by *Einstein Probe* that subsequently triggered coordinated observations across various wavelengths.

3.2. Notable Sources

During its first year of operation, *EP* detected numerous interesting X-ray transients. Here, we highlight five of them.

The first transient detected by *EP* was EPW20240219aa, reported during its commissioning phase [19]. Follow-up analysis suggested that this source was likely a gamma-ray burst (GRB) event, based on the detection of a coincident weak gamma-ray transient in *Fermi*/GBM data [20]. This source was subsequently identified as an untriggered gamma-ray burst through archival searches in *Fermi*/GBM, *Swift*/BAT, and *Insight*-HXMT/HE data. The joint spectral analysis revealed that a single cutoff power-law model could well describe both X-ray and gamma-ray bands, with a photon index of -1.70 ± 0.05 and a peak energy of 257 ± 134 keV, classifying it as an X-ray rich GRB. The analysis of prompt emission suggested a Poynting flux-dominated outflow rather than a thermal photon-dominated one. While follow-up observations in optical and radio bands identified several candidates, none was confirmed as the afterglow counterpart [21]. This discovery not only marked *EP*'s first light but also demonstrated its capability in detecting and characterizing the soft X-ray emission of GRBs.

A particularly remarkable discovery was EP240315a, detected on 15 March 2024, which represents one of the most distant high-energy transients observed by *EP*, at a redshift of $z = 4.859$ [22]. This event exhibited strikingly different temporal profiles between its soft X-ray and gamma-ray emissions—while the gamma-ray emission observed by *Swift*/BAT and *Konus*-Wind lasted approximately 40 s, the soft X-ray emission detected by *EP*-WXT persisted for over 1000 s, making it one of the longest GRB durations ever measured [23]. High-redshift GRBs provide crucial insights into the early universe, serving as beacons to probe the formation of the first-generation stars and the reionization epoch. EP240315a joins this class, which includes GRB 090423 ($z = 8.2$) [5,24], further extending the sample of high-redshift bursts accessible to soft X-ray observations. Multi-wavelength follow-up observations revealed a relativistic jet with a half-opening angle of approximately 3° and a beaming-corrected total energy of $\sim 4 \times 10^{51}$ erg, typical of long GRBs [25]. The optical counterpart was detected by ATLAS approximately 1.3 h after the initial X-ray trigger, showing rapid fading behavior with a decay of $\sim$2 magnitudes within 19 h, while the radio counterpart was detected 2.86 days post-burst using the MeerKAT radio telescope, revealing emission consistent with optically thick synchrotron radiation. The combination of multi-wavelength observations suggested EP240315a originated from a highly relativistic event, likely either a long gamma-ray burst or a jetted tidal disruption event, and demonstrated that some FXTs could be related to the lower-luminosity end of the GRB population [26]. This discovery highlights *EP*'s capability to probe the high-redshift transient universe,

complementing existing missions and potentially uncovering the population of early-universe X-ray transients.

Another intriguing discovery was EP240408a, detected on 8 April 2024, which represents a new class of X-ray transients with an intermediate timescale [27]. The source exhibited a peculiar light curve featuring a 12 s intense X-ray flare that reached a peak flux of 3.9×10^{-9} erg cm^{-2} s^{-1} in the 0.5–4 keV energy band, approximately 300 times brighter than its underlying emission [27]. Further analysis revealed that at redshift z > 0.5, this corresponds to a peak luminosity of $\sim 10^{49}$ erg s^{-1} [11]. The X-ray emission showed a plateau phase lasting for 4 days with luminosity exceeding 10^{46} erg s^{-1}, followed by a steep decay ($\propto t^{-7}$) [11]. Extensive multi-wavelength follow-up observations revealed no optical or radio counterparts, though a faint potential host galaxy (r $\sim$ 24 AB mag) was identified near the X-ray localization [11]. The source's X-ray spectrum remained non-thermal throughout the outburst, with a power-law photon index varying between 1.8–2.5 [27]. The observed properties of EP240408a were found to be inconsistent with known transient types—notably, the lack of a bright gamma-ray counterpart conflicts with typical gamma-ray bursts of similar X-ray luminosities, suggesting it may represent either a peculiar jetted tidal disruption event at z > 1.0 or an entirely new class of X-ray transients [11].

EP240414a, discovered on 14 April 2024, represents a highly unique fast X-ray transient. Located at a redshift of $z = 0.4018$, it showed an unusually large offset (approximately 26–27 kpc) from its spiral host galaxy [28]. The source exhibited a complex, multi-component light curve featuring an initial rapid decline, followed by an unusual re-brightening reaching an absolute magnitude $M_r \sim -21$ after two rest-frame days [29]. In the radio band, the source peaked around 30 days post-explosion with luminosity comparable to long gamma-ray bursts ($\sim 2 \times 10^{30}$ erg s^{-1} Hz^{-1}), indicating a moderately relativistic outflow (bulk Lorentz factor $\Gamma \gtrsim 1.6$) [30]. The source eventually revealed a broad-lined Type Ic supernova component, and while it shared some characteristics with luminous fast blue optical transients (LFBOTs), its distinctive red colors and high X-ray luminosity ($\sim 10^{48}$ erg s^{-1}) suggested different physical mechanisms [31]. This remarkable source represents a previously unknown population of extragalactic fast X-ray transients, bridging the gap between classical gamma-ray bursts and ordinary stripped-envelope supernovae.

EP240709a, discovered by *EP* on 9 July 2024, represents a distinctive blazar candidate exhibiting remarkable characteristics. Its most notable feature is an extraordinary orphan X-ray flare, where the flux in the 0.5–10 keV energy band increased by at least 28 times compared to its low state in 2020, while showing no significant variability in radio, infrared, optical, UV, and GeV bands [32]. Subsequent NICER monitoring revealed X-ray flux variations between $(3-9) \times 10^{-12}$ erg s^{-1} cm^{-2} in the 0.4–3.0 keV band, and multiple lines of evidence support its classification as a high-frequency-peaked BL Lac object, including its spatial coincidence with the Fermi unassociated source 4FGL J0031.5-5648 and a 99.98% probability of being a quasar as revealed by *Gaia* DR3 machine learning classification [33]. This discovery demonstrates *Einstein Probe*'s capability in identifying peculiar activities from active galactic nuclei through high-cadence X-ray sky surveys.

4. Conclusions

The first year of *Einstein Probe* (*EP*) operations has not only validated its unique capabilities in monitoring the dynamic X-ray sky but also yielded critical insights into high-energy transient phenomena, thanks to the capability of rapidly disseminating high-energy alerts associated with early follow-up observations, such as the ones carried out with our BOOTES network.

Out of the 128 events, the BOOTES network has been able to follow up on 58 events, detecting 6 optical counterparts at early times (EP240309a, EP trigger ID 01708981728, EP240804a, EP241109a, GRB 241105A, and EP trigger ID 01709128948).

While *EP* delivered outstanding results in its inaugural year, continued improvements in data processing, calibration, and real-time alert dissemination will further enhance its scientific yield. Moreover, coordinated multi-wavelength and multi-messenger follow-up observations remain essential for fully characterizing the diverse transient phenomena uncovered by *EP*. In this regard, we expect the early-time follow-up by the BOOTES Global Network (and other facilities) will enhance the overall picture of the transients discovered by *EP*.

As time-domain and multi-messenger astronomy continue to evolve, *EP*'s first-year contributions firmly establish it as a key observatory for unveiling the transient X-ray universe, effectively bridging the gap between current and next-generation high-energy missions.

Author Contributions: S.W., A.J.C.-T., and Y.H.: methodology, formal analysis, and investigation; I.P.-G., M.G., M.D.C.-G., S.G., E.J.F.-G., and R.S.-R.: resources, data curation; Y.H., M.G., A.J.C.-T., C.P.-d.-P., G.G.S., D.X., and B.-B.Z.: supervision; A.J.C.-T. and M.G.: funding acquisition; S.W.: writing—original draft preparation; all authors: writing—review and editing. All authors have read and agreed to the published version of the manuscript.

Funding: This work was supported by the China Scholarship Council (CSC). We acknowledge the use of data from the BOOTES (Burst Observer and Optical Transient Exploring System) network. We thank the Instituto de Astrofísica de Andalucía (IAA-CSIC) for its support and collaboration in this research. A.J.C.-T. acknowledges funding from the Spanish Ministry of Science, Innovation and Universities through project PID2023-151905OB-I00, and the Centro de Excelencia Severo Ochoa grant CEX2021-001131-S, funded by MCIN/AEI/10.13039/501100011033. M.G. acknowledges support from the Academy of Finland project No. 325806. The research at Ural Federal University (UrFU) was supported by the Priority-2030 development program (04.89).

Data Availability Statement: The data supporting this study are available from the corresponding author(s) upon reasonable request. Additionally, part of the data used in this work were obtained from publicly available sources, including Gamma-ray Coordinates Network (GCN) Circulars (https://gcn.nasa.gov/circulars, accessed on 26 February 2025), The Astronomer's Telegram (ATel) (https://www.astronomerstelegram.org, accessed on 26 February 2025), and previously published research. Readers are encouraged to refer to these sources for further details.

Acknowledgments: We thank the Instituto de Astrofísica de Andalucía (IAA-CSIC) for its institutional support and collaboration in this research. We also acknowledge the contributions of the BOOTES team for their assistance in data collection and technical support. We are grateful to the GCN and ATel communities for providing timely alerts and observational data, which greatly benefited this study. Additionally, we appreciate the observational efforts of various ground-based facilities. The authors also extend their gratitude to colleagues who provided valuable discussions and feedback during the development of this work. We further thank the EP team for fruitful conversations that provided valuable insights and enriched this work.

Conflicts of Interest: The authors declare no conflicts of interest. The funders had no role in the design of the study; in the collection, analyses, or interpretation of data; in the writing of the manuscript; or in the decision to publish the results.

Abbreviations

The following abbreviations are used in this manuscript:

EP	Einstein Probe
WXT	Wide-field X-ray Telescope
FXT	Follow-up X-ray Telescope
FXTs	Fast X-ray Transients
SVOM	Space-based multi-band astronomical Variable Objects Monitor
BOOTES	Burst Observer and Optical Transient Exploring System
GCN	Gamma-ray Coordinates Network
TDE	Tidal Disruption Event
GRB	Gamma-Ray Burst
ATel	The Astronomer's Telegram
NICER	Neutron star Interior Composition Explorer
eROSITA	extended Roentgen Survey with an Imaging Telescope Array
Chandra	Chandra X-Ray Observatory
XRT	X-ray Telescope
BAT	Burst Alert Telescope
GBM	Gamma-ray Burst Monitor
ROSAT	Roentgen Satellite
AGN	Active Galactic Nucleus
CV	Cataclysmic Variable
HMXB	High-Mass X-ray Binary
APEC	Astrophysical Plasma Emission Code
SDSS	Sloan Digital Sky Survey
WFCAM	Wide Field Camera
VISTA	Visible and Infrared Survey Telescope for Astronomy
VLT	Very Large Telescope
GTC	Gran Telescopio Canarias
OSIRIS	Optical System for Imaging and low-Intermediate-Resolution Integrated Spectroscopy
UCAC4	U.S. Naval Observatory CCD Astrograph Catalog, 4th edition
Gaia DR3	Gaia Data Release 3

Appendix A

Table A1. Multi-wavelength follow-up observations of Einstein Probe transients.

Name	Optical/NIR	X-Ray/Gamma-Ray	Radio/mm
EPW20240219aa	REM, LDT, NIRES, WINTER, Xinglong Observatory, GECKO/LOAO, 7DT, Mondy, Liverpool	SPI-ACS/INTEGRAL, Insight-HXMT/HE, Swift BAT, Fermi GBM	VLA
EP240305a	SALT, GRANDMA	Swift	ATCA
EP240309a	SALT	–	MeerKAT
EP240315a	WIRC, Ondřejov Observatory (D50), GTC, PRIME, 3.6 m TNG NIR, TShAO (Zeiss-1000), Kitab, Montarrenti, Lulin observatory, GROND J-band, VLT/X-shooter, Nanshan/HMT, Liverpool Telescope, ATLAS, Kinder	Chandra, Konus-Wind, Swift/BAT	e-MERLIN, ATCA, MeerKAT

Table A1. *Cont.*

Name	Optical/NIR	X-Ray/Gamma-Ray	Radio/mm
EP240331a	BOOTES-6, 7, MASTER, GRANDMA, Kinder	–	
LXT 240402A	VLT X-shooter, WFST, AST3-3, MASTER, GWAC-F50A, Kinder	LEIA, Chandra, Swift, Konus-Wind, GECAM-C, Glowbug, Fermi GBM	MeerKAT, ATCA, e-Merlin
EP240408a	BOOTES-2, 4, GSP, MASTER, GROND,	GECAM-B, *Swift*-XRT	–
EP240413a	BOOTES-5, GOTO	GECAM-B	–
EP240414a	BOOTES-2, GTC, LBT, Gemini-South, NIRES, WINTER, Terskol Zeiss-2000, GMG, GSP, Pan-STARRS, Kinder	Chandra	MeerKAT
EP240416a	WINTER, Terskol Zeiss-2000, Khureltogoot, BOOTES-2/TELMA, MASTER, Kinder	–	–
EP240417a	BOOTES-5, YAHPT, SOAR	–	–
EP240420a	BOOTES-6, TNT, Xinglong, Nanshan, GWAC-F50A, NOT	–	–
EP240426a	BOOTES-6, GMG-2.4 m, DECam	EP-FXT	ASKAP, VAST
EP240426b	AST3-2	–	–
EP240506a	BOOTES-2, 5, 6, 7, Xinglong, CrAO ZTSH, TRT, BOOTES Network, Kinder	–	RACS, VLASS
EP240518a	BOOTES-4, 6, GSP	–	–
EP240617a	BOOTES-6, 7, STEP/T80S	Swift/XRT, Fermi/GBM	–
EP240618a	BOOTES-6, 7, NOT, GSP, Abastumani, GRANDMA, TRT, OHP/T193 MISTRAL	Fermi/GBM, Swift/XRT	–
EP240625a	BOOTES-5, 6, 7, GRANDMA, NOT	–	–
EP240626a	BOOTES-7, Montarrenti Observatory, KAIT	–	–
EP240702a	BOOTES-6,7, 7DT, TRT, GSP	Swift/XRT	–
EP240703a	BOOTES-6, TRT, KAIT, BTA, Liverpool Telescope, Kinder, JinShan	Konus-Wind, Swift/XRT	–
EP240703b	GSP, TRT	Swift/XRT	–
EP240703c	Kinder	Swift/XRT	–
EP240708a	BOOTES-6,7, Kinder, GSP, KAIT, NOT, SVOM/C-GFT	Swift/XRT	–
EP240801a	BOOTES-5, 6, 7, GTC, Keck/LRIS, Assy-Turgen, BTA BVRI, ZTSh (CrAO), Osservatorio Astronomico Nastro Verde, SAO RAS, CrAO, AbAO, GRANDMA, Kilonova-Catcher, Leavitt Observatory, JinShan, NOT, LCOGT, GSP, Kinder, KAIT, GMG, TRT	–	GMRT

Table A1. *Cont.*

Name	Optical/NIR	X-Ray/Gamma-Ray	Radio/mm
EP240802a	Kinder, SWIFT-UVOT, KAIT, Montarrenti Observatory, Bassano Bresciano Observatory	SWIFT-XRT, Konus-Wind, SVOM/GRM	–
EP240804a	LCOGT, BOOTES-6, NOT, GSP, VLT/X-shooter, LCOGT	Konus-Wind	–
EP240806a	BOOTES-6, 7, Global MASTER, Liverpool Telescope, Gemini North-GMOS, KAIT, LCOGT, GSP	–	–
EP240807a	BOOTES-6, 7, PRIME, STEP/T80S, Global MASTER	Konus-Wind	–
EP240816a	BOOTES-6, 7, Liverpool Telescope, KAIT, Global MASTER, TRT	–	–
EP240816b	BOOTES-6, 7, TRT, MASTER, KAIT, Liverpool	–	–
EP240820a	BOOTES-6, 7, PRIME, TRT	–	–
EP240904a	NOT	NuSTAR	ATCA
EP240908a	Gemini-North telescope, Mondy, AbAO, optical afterglow candidate, Global MASTER, TRT	WXT, FXT	–
EP240913a	AbAO, Mephisto, MASTER, VLT/HAWK-I, KAIT, NOT, JinShan, ESO-NTT	–	–
EP240918a	SVOM/VT, 1.6 m Mephisto, Global MASTER, JinShan, YAHPT, Kinder, GMG	Swift/XRT	–
EP240918b	Kinder	–	–
EP240918c	Kinder	–	–
EP240919a	BOOTES-6, 7, SVOM/VT, Mondy, REM, KAIT, Kinder, Global MASTER, NOT, Gemini, GOTO, JinShan	Fermi GBM, SVOM/GRM, INTEGRAL SPI-ACS	–
EP240930a	KAIT, CrAO ZTSH, SVOM/C-GFT, Liverpool Telescope, GOTO, Global MASTER	IPN triangulation, Swift/BAT	–
EP241021a	GTC, OSN, CAHA, Keck/LRIS, OHP/T193, SOAR, Kinder, Liverpool Telescope, Mephisto, SAO RAS, Gemini-South, Xinglong Observatory, Fraunhofer Telescope, VLT/FORS2, KAIT, DFOT, GSP, TRT, NOT, MASTER, GOTO	Konus-Wind, Swift-UVOT, Fermi-GBM	SMA, VLA, AMI-LA, ATCA, e-MERLIN
EP241025a	TNT, TRT	–	–
EP241026b	Keck/LRIS, Kinder, Liverpool Telescope, LBT, GROWTH, MASTER	–	–
EP241030a	Kinder, TNOT, SAO RAS, GMG, FTW, MASTER	–	–

Table A1. *Cont.*

Name	Optical/NIR	X-Ray/Gamma-Ray	Radio/mm
EP241101a	BOOTES-4, 7, CrAO ZTSH, NUTTelA-TAO/BSTI, FTW, Kinder, OHP/T193, MASTER,	–	–
EP241103a	BOOTES-4, 7, GTC, GIT, GOTO, Gemini, GSP, LCO, MASTER	Swift XRT	–
EP241104a	Kinder	–	–
EP241107a	BOOTES-7, OSN, CAHA, GTC, SOAR, AbAO, MASTER, KAIT, Kinder, AKO, GSP, Gemini-South, OHP/T193, FTW, GIT, MASTER, SVOM/C-GFT, AKO	–	VLA
EP241109a	KAIT, Lick, BOOTES-5, 7	–	–
EP241113a	BOOTES-4, OSN, Keck/LRIS, MASTER, WINTER	Swift XRT, Fermi-GBM	eMERLIN
EP241113b	OSN, Global MASTER	–	–
EP241115a	CAHA, Kinder, MASTER	Swift XRT, SVOM/GRM	–
EP241119a	BOOTES-4, 5, 7, 7DT, Kinder, GIT, WINTER, MASTER	–	–
EP241125a	BOOTES-b1b, 4, 5, 7, Kinder	–	–
EP241126a	BOOTES-7, SOAR, Mephisto, NOT, SVOM/VT, WFST, Kinder, GSP, TRT	–	–
EP241201a	BOOTES-4, 5, GTC, Mephisto, Kinder, NOT, MASTER	–	–
EP241202b	BOOTES-4, 5, 7, MASTER, KAIT	Fermi-GBM	–
EP241206a	MASTER, BOOTES, OSN	–	–
EP241208a	BOOTES-4, 7, OSN, MASTER, NOT, Kinder	SVOM/ECLAIRs	–
EP241213a	–	GRBAlpha, Konus-Wind, INTEGRAL/SPI-ACS	–
EP241217a	BOOTES-4, 6, OSN, GTC, SYSU, Liverpool, Leavitt, Mephisto, REM, NOT, GROWTH, Xinglong, MASTER, Gemini-North, Kinder, LCO	Fermi-GBM, Swift-XRT	–
EP241217b	Mephisto, GRANDMA/T1MPicduMidi, Nanshan/HMT, NOT, REM, SOAR, MASTER	Fermi-GBM	VLA, ATCA
EP241223a	BOOTES-4, 7, Mondy AZT-33IK, MASTER	–	–
EP241231b	Liverpool	–	–
EP250101a	Xinglong, Liverpool	–	–
EP250108a	BOOTES-4, 6, CAHA, AbAO, CMO, Terskol, DFOT, Gemini GMOS-S, NOT, GMG, SAO RAS, Mephisto, LCO, Liverpool Telescope, MASTER, VLT/X-shooter	Swift/XRT, Fermi-GBM	ATCA, VLA, MeerKAT

Table A1. *Cont.*

Name	Optical/NIR	X-Ray/Gamma-Ray	Radio/mm
EP250109a	Mephisto, SVOM/VT, Terskol (INASAN), SAO RAS, GMG, MASTER, GOTO	GRBAlpha, Swift/BAT-GUANO, Swift/XRT, Swift/UVOT, Fermi-GBM	–
EP250109b	Liverpool	–	–
EP250111a	BOOTES-5, GTC, SAO RAS, KAIT, Mondy, NOT, MASTER	Einstein Probe WXT, Swift/XRT	–
EP250125a	BOOTES-7, DFOT, Kinder, Gemini, REM	Fermi, Swift	–
EP250205a	FTW	–	VLA
EP250207a	BOOTES-6, 7, NOT	Fermi-GRB, XRT	–
EP250207b	BOOTES-5, GTC, Xinglong, NOT, Liverpool, MASTER, Gemini	Chandra	VLA
EP250212a	FTW, Xinglong, MASTER, Liverpool, NOT	–	–
EP250215a	GTC, LCO, COLIBRI, NOT, Mephisto, Gemini, SVOM, MASTER	AstroSat CZTI, INTEGRAL SPI-ACS	–
EP250220a	FTW, Liverpool Telescope, Mephisto, Kinder, Xinglong, MASTER	–	–
EP250223a	BOOTES-4, CraO ZTSH, GMG, GROWTH-India, Kinder, GOTO, COLIBRI/DDRAGO, REM, TRT, Mephisto, SVOM/VT, OASDG, LCO, NOT, MASTER	Swift/XRT	–
EP250226a	Xinglong, SVOM/VT, Mephisto, Kinder, GSP, COLIBRI/DDRAGO, VLT/X-shooter, TRT, MASTER	INTEGRAL SPI-ACS and PICsIT, GECAM-B	–

References

1. Remillard, R.A.; McClintock, J.E. X-Ray Properties of Black-Hole Binaries. *Annu. Rev. Astron. Astrophys.* **2006**, *44*, 49–92. [CrossRef]
2. Komossa, S. Tidal disruption of stars by supermassive black holes: Status of observations. *J. High Energy Astrophys.* **2015**, *7*, 148–157. [CrossRef]
3. Kumar, P.; Zhang, B. The physics of gamma-ray bursts & relativistic jets. *Phys. Rep.* **2015**, *561*, 1–109. [CrossRef]
4. Abbott, B.P.E.A. Multi-messenger Observations of a Binary Neutron Star Merger. *Astrophys. J. Lett.* **2017**, *848*, L12. [CrossRef]
5. Salvaterra, R.; Della Valle, M.; Campana, S.; Chincarini, G.; Covino, S.; D'Avanzo, P.; Fernandez-Soto, A.; Guidorzi, C.; Tagliaferri, G.; Antonelli, L.A.; et al. GRB 090423 at a redshift of z 8.1. *Nature* **2009**, *461*, 1258–1260. [CrossRef]
6. Yuan, W. The Einstein Probe mission. In Proceedings of the 44th COSPAR Scientific Assembly, Online, 16–24 July 2022; Abstract E1.16-0036-22.
7. Yuan, W.; Dai, L.; Feng, H.; Jin, C.; Jonker, P.; Kuulkers, E.; Liu, Y.; Nandra, K.; O'Brien, P.; Piro, L.; et al. Science objectives of the Einstein Probe mission. *Sci. China Phys. Mech. Astron.* **2025**, *68*, 239501. . [CrossRef]
8. Castro-Tirado, A.J.; Soldán, J.; Bernas, M.; Páta, P.; Rezek, T.; Hudec, R.; Sanguino, T.M.; de la Morena, B.; Berná, J.A. The Burst Observer and Optical Transient Exploring System (BOOTES). *Astron. Astrophys. Suppl. Ser.* **1999**, *138*, 583–585. [CrossRef]
9. Hu, Y.D.; Castro-Tirado, A.J.; Fernández-García, E.; Caballero-García, M.D.; Pérez-García, I.; Carrasco-García, I.M.; Castellón, A.; Pérez del Pulgar, C.; Reina Terol, A.J. The Burst Observer and Optical Transient Exploring System in the Multi-messenger Astronomy Era. *Front. Astron. Space Sci.* **2023**, *10*, 952887. [CrossRef]
10. Castro-Tirado, A.J. Tracking transients night and day. *Nat. Astron.* **2023**, *7*, 1136. [CrossRef]
11. O'Connor, B.; Pasham, D.; Andreoni, I.; Hare, J.; Beniamini, P.; Troja, E.; Ricci, R.; Dobie, D.; Chakraborty, J.; Ng, M.; et al. Characterization of a peculiar Einstein Probe transient EP240408a: An exotic gamma-ray burst or an abnormal jetted tidal disruption event? *arXiv* **2024**, arXiv:2410.21622. [CrossRef]

12. Caballero-García, M.D.; Jelínek, M.; Castro-Tirado, A.J.; Hudec, R.; Cunniffe, R. Initial follow-up of optical transients with COLORES using the BOOTES network. *Acta Polytech.* **2015**, *55*, 81–85. [CrossRef]
13. Chambers, K.C.; Magnier, E.A.; Metcalfe, N.; Flewelling, H.A.; Huber, M.E.; Waters, C.Z.; Denneau, L.; Draper, P.W.; Farrow, D.; Finkbeiner, D.P.; et al. The Pan-STARRS1 Surveys. *arXiv* **2016**, arXiv:1612.05560. . [CrossRef]
14. Caballero-García, M.D.; Simon, V.; Jelínek, M.; Castro-Tirado, A.J.; Cwiek, A.; Claret, A.; Opiela, R.; Żarnecki, A.F.; Gorosabel, J.; Oates, S.R.; et al. Early optical follow-up of the nearby active star DG CVn during its 2014 superflare. *Mon. Not. R. Astron. Soc.* **2015**, *452*, 4195–4202. [CrossRef]
15. Kreps, J.; Narkhede, N.; Rao, J. Kafka: A Distributed Messaging System for Log Processing. In Proceedings of the 6th International Workshop on Networking Meets Databases, Athens, Greece, 12 June 2011.
16. Antognini, J.M.O. Timescales of Kozai–Lidov oscillations at quadrupole and octupole order in the test particle limit. *Mon. Not. R. Astron. Soc.* **2015**, *452*, 3610–3619. [CrossRef]
17. Kouveliotou, C.; Meegan, C.A.; Fishman, G.J.; Bhat, N.P.; Briggs, M.S.; Koshut, T.M.; Paciesas, W.S.; Pendleton, G.N. Identification of two classes of gamma-ray bursts. *Astrophys. J.* **1993**, *413*, L101. [CrossRef]
18. Sguera, V.; Barlow, E.J.; Bird, A.J.; Dean, A.J.; Landi, R.; Lubinski, P.; Malizia, A.; Ubertini, P. INTEGRAL observations of recurring fast X-ray transients. *Astron. Astrophys.* **2005**, *444*, 221–231. [CrossRef]
19. Zhang, C.; Ling, Z.X.; Liu, Y.; Pan, X.; Jin, C.; Cheng, H.Q.; Cui, C.Z.; Fan, D.W.; Hu, H.B.; Hu, J.W.; et al. *Detection of a Bright X-Ray Flare by Einstein Probe in Its Commissioning Phase*; Astronomer's Telegram, No. 16463; Harvard University: Cambridge, MA, USA, 2024.
20. Zhang, B.; Sun, H.; Yin, Y.H.I.; Yang, J.; Zhang, B.; Wu, X. *EPW20240219aa Is Likely a GRB Event*; Astronomer's Telegram, No. 16473; Harvard University: Cambridge, MA, USA, 2024.
21. Yin, Y.H.I.; Zhang, B.B.; Yang, J.; Sun, H.; Zhang, C.; Shao, Y.X.; Hu, Y.D.; Zhu, Z.P.; Xu, D.; An, L.; et al. Triggering the Untriggered: The First Einstein Probe-Detected Gamma-Ray Burst 240219A and Its Implications. *arXiv* **2024**, arXiv:2407.10156. [CrossRef]
22. Liu, Y.; Sun, H.; Xu, D.; Svinkin, D.S.; Delaunay, J.; Tanvir, N.R.; Gao, H.; Zhang, C.; Chen, Y.; Wu, X.F.; et al. Soft X-ray prompt emission from a high-redshift gamma-ray burst EP240315a. *arXiv* **2024**, arXiv:2404.16425. [CrossRef]
23. Levan, A.J.; Jonker, P.G.; Saccardi, A.; Malesani, D.B.; Tanvir, N.R.; Izzo, L.; Heintz, K.E.; Sánchez, D.M.; Quirola-Vásquez, J.; Torres, M.A.; et al. The fast X-ray transient EP240315a: A z 5 gamma-ray burst in a Lyman continuum leaking galaxy. *arXiv* **2024**, arXiv:2404.16350.
24. Tanvir, N.R.; Fox, D.B.; Levan, A.J.; Berger, E.; Wiersema, K.; Fynbo, J.P.U.; Cucchiara, A.; Krühler, T.; Perley, D.A.; Cenko, S.B.; et al. A γ-ray burst at a redshift of $z \sim 8.2$. *Nature* **2009**, *461*, 1254–1257. [CrossRef]
25. Ricci, R.; Troja, E.; Yang, Y.H.; Yadav, M.; Liu, Y.; Sun, H.; Wu, X.; Gao, H.; Zhang, B.; Yuan, W. Long-term radio monitoring of the fast X-ray transient EP240315a: Evidence for a relativistic jet. *arXiv* **2024**, arXiv:2407.18311.
26. Gillanders, J.H.; Rhodes, L.; Srivastav, S.; Carotenuto, F.; Bright, J.; Huber, M.E.; Stevance, H.F.; Smartt, S.J.; Chambers, K.C.; Chen, T.W.; et al. Discovery of the optical and radio counterpart to the fast X-ray transient EP240315a. *arXiv* **2024**, arXiv:2404.10660.
27. Zhang, W.; Yuan, W.; Ling, Z.; Chen, Y.; Rea, N.; Rau, A.; Cai, Z.; Cheng, H.; Zelati, F.C.; Dai, L.; et al. Einstein Probe discovery of EP240408a: A peculiar X-ray transient with an intermediate timescale. *Sci. China Phys. Mech. Astron.* **2024**, *68* , 219511. [CrossRef]
28. Sun, H.; Li, W.X.; Liu, L.D.; Gao, H.; Wang, X.F.; Yuan, W.; Zhang, B.; Filippenko, A.V.; Xu, D.; An T.; et al. Extragalactic fast X-ray transient from a weak relativistic jet associated with a Type Ic-BL supernova. *arXiv* **2025**, arXiv:2410.02315.
29. Srivastav, S.; Chen, T.W.; Gillanders, J.H.; Rhodes, L.; Smartt, S.J.; Huber, M.E.; Aryan, A.; Yang, S.; Beri, A.; Cooper, A.J.; et al. Identification of the optical counterpart of the fast X-ray transient EP240414a. *Astrophys. J. Lett.* **2025**, *978*, L21. [CrossRef]
30. Bright, J.S.; Carotenuto, F.; Fender, R.; Choza, C.; Mummery, A.; Jonker, P.G.; Smartt, S.J.; DeBoer, D.R.; Farah, W.; Matthews, J.; et al. The Radio Counterpart to the Fast X-ray Transient EP240414a. *arXiv* **2024**, arXiv:2409.19055. [CrossRef]
31. van Dalen, J.N.; Levan, A.J.; Jonker, P.G.; Malesani, D.B.; Izzo, L.; Sarin, N.; Quirola-Vásquez, J.; Sánchez, D.M.; de Ugarte Postigo, A.; van Hoof, A.P.; et al. The Einstein Probe transient EP240414a: Linking Fast X-ray Transients, Gamma-ray Bursts and Luminous Fast Blue Optical Transients. *Astrophys. J. Lett.* **2025**, *982*, L47. [CrossRef]
32. Liu, M.; Zhang, Y.; Wang, Y.; Xue, R.; Buckley, D.; Howell, D.A.; Jin, C.; Li, W.; Monageng, I.; Pan, H.; et al. Detection of an Orphan X-ray Flare from a Blazar Candidate EP240709a with Einstein Probe. *arXiv* **2024**, arXiv:2412.18463. [CrossRef]
33. Ng, M.; Hare, J.; Jaisawal, G.K.; Malacaria, C.; Markwardt, C.B.; Sanna, A. Tentative Blazar Candidate EP240709A Associated with 4FGL J0031.5-5648: NICER and Archival Multiwavelength Observations. *arXiv* **2024**, arXiv:2411.18718. [CrossRef]